Part I

The Energetics of Cosmic Explosions

CHAPTER 2

A Jet Model for the Afterglow Emission from GRB 000301C†

E. Berger[a], R. Sari[b], D. A. Frail[c], S. R. Kulkarni[a], F. Bertoldi[d], A. B. Peck[d], K. M. Menten[d], D. S. Shepherd[c], G. H. Moriarty-Schieven[e], G. Pooley[f], J. S. Bloom[a], A. Diercks[a], T. J. Galama[a], & K. Hurley[g]

[a]Department of Astronomy, 105-24 California Institute of Technology, Pasadena, CA 91125, USA

[o]Theoretical Astrophysics 130-33, California Institute of Technology, Pasadena, CA 91125

[c]National Radio Astronomy Observatory, Socorro, NM 87801

[d]Max-Planck-Institut fr Radioastronomie, Auf dem Huegel 69, D-53121 Bonn, Germany

[e]Joint Astronomy Centre, 660 N. A'ohoku Place, Hilo, HI 96720

[f]Mullard Radio Astronomy Observatory, Cavendish Laboratory, Madingley Road, Cambridge CB3 0HE, England UK

[g]University of California at Berkeley, Space Sciences Laboratory, Berkeley, CA 94720

Abstract

We present broad-band radio observations of the afterglow of GRB 000301C, spanning from 1.4 to 350 GHz for the period of $3 - 130$ days after the burst. These radio data, in addition to measurements in the optical bands, suggest that the afterglow arises from a collimated outflow, i.e., a jet. To test this hypothesis in a self-consistent manner, we employ a global fit and find that a model of a jet expanding into a constant-density interstellar medium (ISM+jet) provides the best fit to the data. A model of the burst occurring in a wind-shaped circumburst medium (wind-only model) can be ruled out, and a wind+jet model provides a much poorer fit of the optical/IR data than the ISM+jet model. In addition, we present the first clear indication that the reported fluctuations in the optical/IR are achromatic, with similar amplitudes in all bands, and possibly extend into the radio regime. Using the parameters derived from the global fit, in particular a jet break time $t_{\rm jet} \approx 7.3$ days, we infer a jet opening angle of $\theta_0 \approx 0.2$ rad; consequently, the estimate of the emitted energy in the GRB itself is reduced by a factor of 50 relative to the isotropic value, giving $E \approx 1.1 \times 10^{51}$ erg.

† A version of this chapter was published in *The Astrophysical Journal*, vol. 545, 56–62, (2000).

SECTION 2.1

Introduction

GRB 000301C is the latest afterglow to exhibit a break in its optical/IR light curves. An achromatic steepening of the light curves has been interpreted in previous events (e.g., Kulkarni et al. 1999a; Harrison et al. 1999; Stanek et al. 1999) as the signature of a jet-like outflow (Rhoads 1999; Sari et al. 1999), produced when relativistic beaming no longer "hides" the nonspherical surface, and when the ejecta undergo rapid lateral expansion. The question of whether the relativistic outflows from gamma-ray bursts (GRBs) emerge isotropically or are collimated in jets is an important one. The answer has an impact on both estimates of the GRB event rate and the total emitted energy – issues that have a direct bearing on GRB progenitor models.

An attempt by Rhoads & Fruchter (2001) to model this break using only the early-time ($t \lesssim 14$ days) optical/IR data has led to a jet interpretation of the afterglow evolution, but with certain peculiar aspects, such as a different jet break time at the R band than at the K$'$ band. However, subsequent papers by Masetti et al. (2000a) and Sagar et al. (2000), with larger optical data sets, pointed out that there are large flux density variations ($\sim 30\%$) on timescales as short as a few hours, superposed on the overall steepening of the optical/IR light curves. While the origin of these peculiar fluctuations remains unknown, it is clear that they complicate the fitting of the optical/IR data, rendering some of the Rhoads & Fruchter (2001) results questionable.

In this paper we take a different approach. We begin by presenting radio measurements of this burst from 1.4 to 350 GHz, spanning a time range from 3 to 130 days after the burst. These radio measurements, together with the published optical/IR data, present a much more comprehensive data set, which is less susceptible to the effects of the short-timescale optical fluctuations. We then use the entire data set to fit a global, self-consistent jet model, and derive certain parameters of the GRB from this model. Finally, we explore the possibility of a wind and wind+jet global fit to the data, and compare our results with the conclusions drawn in the previous papers.

SECTION 2.2

Observations

Radio observations were made from 1.43 to 350 GHz at a number of facilities, including the James Clark Maxwell Telescope (JCMT[1]), the Institute for Millimeter Radioastronomy (IRAM[2]), the Owens Valley Radio Observatory Interferometer (OVRO), the Ryle Telescope, and the Very Large Array (VLA[3]). A log of these observations and the flux density measurements are summarized in Table 2.1. With the exception of IRAM, we have detailed our observing and calibration methodology in Kulkarni et al. (1999a), Kulkarni et al. (1999b), Frail et al. (2000a), and Frail et al. (2000b).

Observations at 250 GHz were made in the standard on-off mode using the Max-Planck Millimeter Bolometer (MAMBO; Kreysa et al. 1998) at the IRAM 30-m telescope on Pico Veleta, Spain. Gain calibration was performed using observations of Mars, Uranus, and Ceres. We estimate the calibration to be accurate to 15%. The source was initially observed on March 4 (Bertoldi 2000) and again on March 5 and 9 under very stable atmospheric conditions, and on March 6 with high atmospheric opacity. From March 24 to 26, the source was briefly reobserved three times for a total on+off integration time of 2000 s, but no signal was detected.

[1] The JCMT is operated by The Joint Astronomy Centre on behalf of the Particle Physics and Astronomy Research Council of the UK, the Netherlands Organization for Scientific Research, and the National Research Council of Canada.

[2] The Institute for Millimeter Radioastronomy (IRAM) is supported by INSU/CNRS (France), MPG (Germany), and IGN (Spain).

[3] The NRAO is a facility of the National Science Foundation operated under cooperative agreement by Associated Universities, Inc. NRAO operates the VLA.

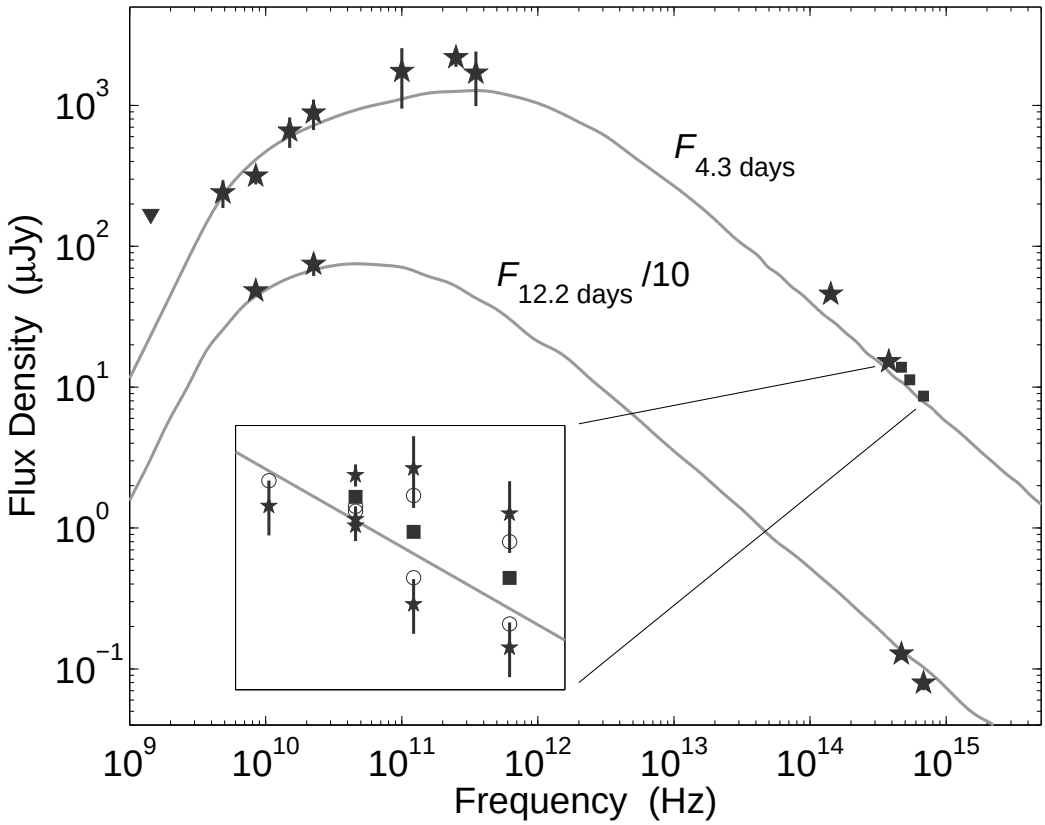

Figure 2.1: Radio to optical spectral flux distribution of GRB 000301C on 2000 March 5.66 UT ($\Delta t \approx 4.26$ days), and 2000 March 13.58 UT ($\Delta t \approx 12.17$ days). The solid lines show the ISM+jet global fit based on a smoothed synchrotron emission spectrum (Granot et al. 1999a,b). The optical/IR data (Masetti et al. 2000a; Sagar et al. 2000; Rhoads & Fruchter 2001) are converted to Jansky flux units (Bessell & Brett 1988; Fukugita et al. 1995), and corrected for Galactic foreground extinction (Schlegel et al. 1998), with $E(B-V) = 0.053$. All data were taken within 0.5 days of the fiducial dates, and the circles show the corrections to the fiducial times, $\Delta t = 4.26$ and 12.17 days. The squares in the optical band show weighted averages of multiple measurements within 1 day of $\Delta t = 4.26$ days (see inset). The data points at 100, 250, and 350 GHz are weighted averages of the individual measurements from around day 4 (see Table 2.1). The data and fit at $\Delta t = 12.17$ days were divided by a factor of ten to avoid overlap with the $\Delta t = 4.26$ curve.

SECTION 2.3

Data

In Figure 2.1 we present broad-band spectra from March 5.66 UT ($\Delta t \approx 4.25$ days) and March 13.58 UT ($\Delta t \approx 12.17$ days). Radio lightcurves at 4.86, 8.46, 22.5, and 250 GHz from Table 2.1 are presented in Figure 2.2, while optical/IR lightcurves are shown in Figure 2.3.

The quoted uncertainties in the flux densities given in Table 2.1 report only measurement error and do not contain an estimate of the effects of interstellar scattering (ISS), which is known to be significant for radio afterglows (e.g., Frail et al. 2000c). We can get some guidance as to the expected magnitude of the ISS-induced modulation of our flux density measurements (in time and frequency) using the models developed by Taylor & Cordes (1993), Walker (1998), and Goodman (1997).

From the Galactic coordinates of GRB 000301C ($l = 48^{\circ}.7$, $b = 44^{\circ}.3$), we find, using the Taylor & Cordes model, that the scattering measure, in units of $10^{-3.5}$, is $SM_{-3.5} \approx 0.7$. The distance to the scattering screen, $d_{\rm scr}$, is one-half the distance through the ionized gas layer, $d_{\rm scr} = (hz/2)(\sin b)^{-1} \approx$

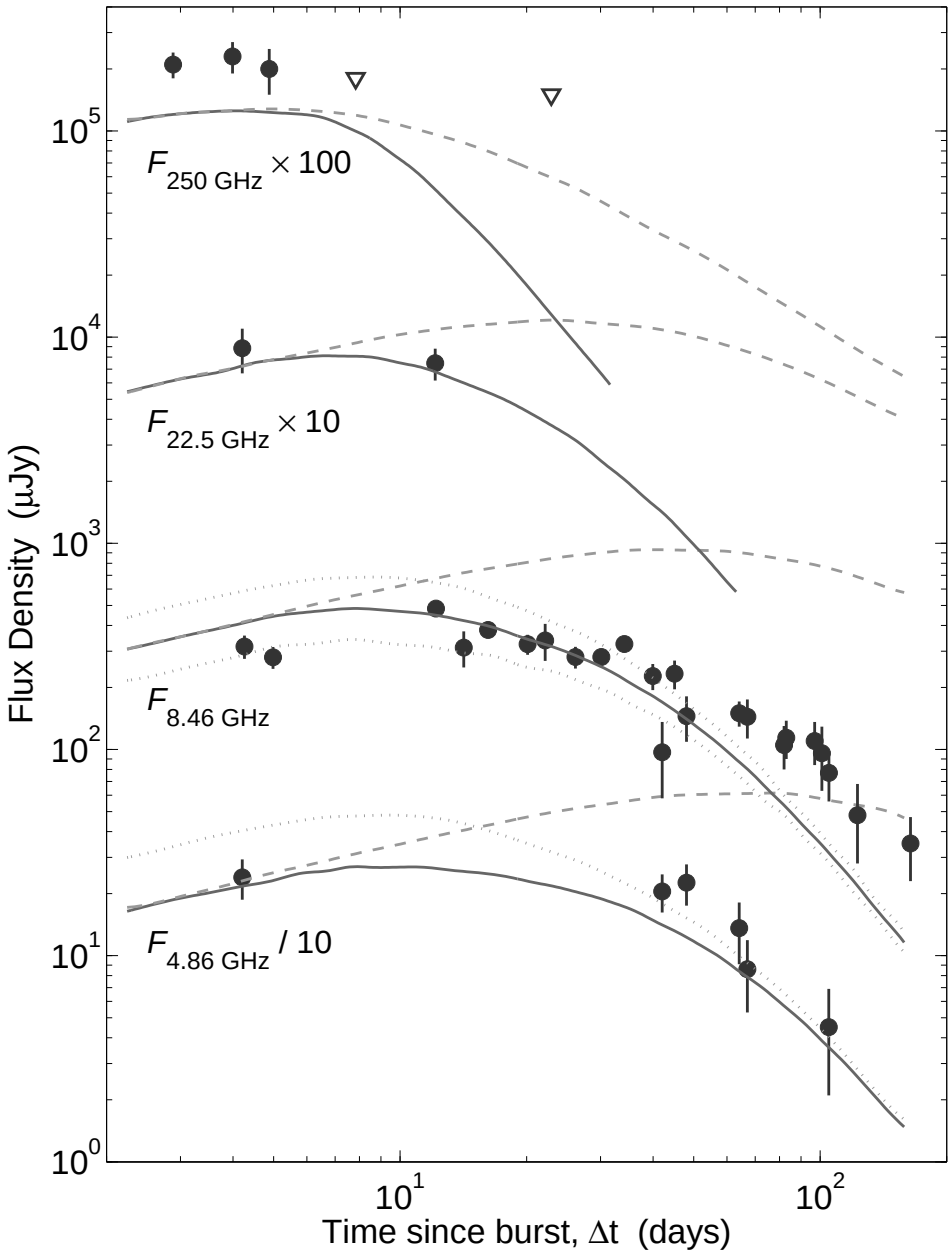

Figure 2.2: Radio lightcurves at 4.86, 8.46, 22.5 and 250 GHz. The solid lines show the ISM+jet model (§2.4). The dashed curve shows the prediction for a spherical evolution of the afterglow (ISM only). The dotted lines indicate the maximum and minimum range of flux expected from ISS (§2.3). Note that the data and fit for 4.86 GHz were divided by a factor of 10, the data and fit for 22.5 GHz were multiplied by a factor of 10, and the data and fit for 250 GHz were multiplied by a factor of 100 to avoid overlap between the four curves.

0.72 kpc, using $hz \approx 1$ kpc. From Walker's analysis, the transition frequency between weak and strong scintillation is then given by $\nu_0 = 5.9 S M_{-3.5}^{6/17} d_{\rm scr}^{5/17} \approx 4.7$ GHz. Goodman (1997) uses the same expression, but with a different normalization for the transition frequency, giving a larger value, $\nu_0 \approx 8.3$ GHz. In this section we follow Walker's analysis, and note that the numbers from Goodman will give somewhat different results.

For frequencies larger than the transition frequency, the modulation index (i.e., the rms fractional flux variation) is $m_\nu = (\nu_0/\nu)^{17/12}$, and the modulation timescale in hours is $t_\nu \approx 6.7 (d_{\rm scr}/\nu)^{1/2}$. From

these equations we find that the modulation index is of the order of 0.4 at 8.46 GHz, 0.2 at 15 GHz, 0.1 at 22.5 GHz, and is negligible at higher frequencies. The modulation timescales are of the order of 2.0 hr at 8.46 GHz, 1.5 hr at 15 GHz, and 1.2 hr at 22.5 GHz. It is important to note that factor of 2 uncertainties in the scattering measure allow the modulation index to vary by $\sim 50\%$.

At these frequencies, the expansion of the fireball will begin to "quench" the ISS when the angular size of the fireball exceeds the angular size of the first Fresnel zone, $\theta_F = 8(d_{\rm scr}\nu_{\rm GHz})^{-1/2}$ μas. To describe the evolution of the source size, θ_s, with time, we have used an expanding jet model (see Frail et al. 2000b), with the factor $(E_{52}/n_1)^{1/8}$ assumed to be of order unity, which gives $\theta_s \approx 3.1(\Delta t_d/15)^{1/2}$ μas; E_{52} is the energy of the GRB in units of 10^{52} erg, n_1 is the density of the circumburst medium in units of 1 cm^{-3}, and Δt_d is the elapsed time since the burst in days. Once the source size exceeds the Fresnel size (after approximately 2 weeks at 8.46 GHz), the modulation index is reduced by a factor $(\Delta t_d/15)^{-7/12}$.

The measurements at 4.86 GHz occur near the transition frequency, and we therefore expect $m_{4.86}$ to be large, $\sim 0.65 - 1$. At 1.43 GHz, the observations were made in the strong regime of ISS, where we expect both refractive and diffractive scintillation. Point-source refractive scintillation at 1.43 GHz has a modulation index $m_{1.43,r} = (\nu/\nu_0)^{17/30} \approx 0.5$, with a timescale of $t_{1.43,r} \approx 2(\nu_0/\nu)^{11/5} \approx 1$ day. The refractive ISS is "quenched" when the angular size of the source is larger than $\theta_r = \theta_{F0}(\nu_0/\nu)^{11/5}$, where θ_{F0} is the angular size of the first Fresnel zone at $\nu_0 = 4.7$ GHz. As with weak scattering, the modulation index must be reduced by a factor $(\Delta t_d/15)^{-7/12}$ after this point. The diffractive scintillation has a modulation index $m_{1.43,d} = 1$ and a timescale $t_{1.43,d} \approx 2(\nu/\nu_0)^{6/5} \approx 0.5$ hr $\ll t_{1.43,r}$. The source can no longer be approximated by a point source when its angular size exceeds $\theta_d = \theta_{F0}(\nu/\nu_0)^{6/5}$, and correspondingly, the modulation index must be corrected by a factor $(\Delta t_d/15)^{-1/2}$.

The redshift of GRB 000301C was measured using the *Hubble Space Telescope* (HST) to be 1.95 ± 0.1 by Smette et al. (2000) and was later refined by Castro et al. (2000) using the Keck II 10-m telescope to a value of 2.0335 ± 0.0003. The combined fluence measured by the GRB detector on board the Ulysses satellite, and the X-ray/gamma-ray spectrometer (XGRS) on board the Near-Earth Asteroid Rendezvous (NEAR) satellite, in the 25-100 keV and > 100 keV bands, was 4.1×10^{-6} erg cm^{-2}. Using the cosmological parameters $\Omega_0 = 0.3$, $\Lambda_0 = 0.7$, and $H_0 = 65$ km s^{-1} Mpc^{-1}, we find that the isotropic γ-ray energy release from the GRB was $E_{\gamma,\rm iso} \approx 5.4 \times 10^{52}$ erg.

SECTION 2.4

A Self-Consistent Jet Interpretation

According to the standard, spherical GRB model, the optical light curves should obey a simple power-law decay, $F_\nu \propto t^{-\alpha}$, with α changing at most by 1/4 as the electrons age and cool (Sari et al. 1998). From Figure 2.3, it is evident that the optical lightcurves steepen substantially ($\Delta\alpha > 1/4$) between days 7 and 8, which indicates that this burst cannot be described within this standard model of an expanding spherical blast wave. This break can be attributed to a jet-like or collimated ejecta (Rhoads 1999; Sari et al. 1999).

The jet model of GRBs predicts the time evolution of flux from the afterglow, and of the parameters $\nu_a \propto t^{-1/5}$, $\nu_m \propto t^{-2}$, and $F_{\nu,\rm max} \propto t^{-1}$, where ν_a is the self-absorption frequency, ν_m is the characteristic frequency emitted by electrons with Lorentz factor γ_m, and $F_{\nu,\rm max}$ is the observed peak flux density. This model holds for $t > t_{\rm jet}$, where $t_{\rm jet}$ is defined by the condition $\Gamma(t_{\rm jet}) \sim \theta_0^{-1}$. Prior to $t_{\rm jet}$, the time evolution of the afterglow is described by a spherically expanding blastwave, with the scalings $\nu_a \propto$ const., $\nu_m \propto t^{-3/2}$, and $F_{\nu,\rm max} \propto$ const. In this paper we designate this model as ISM+jet. Throughout the analysis we assume that the cooling frequency, ν_c, lies above the optical band for the entire time period under discussion in this paper.

At any point in time, the spectrum is roughly given by the broken power law $F_\nu \propto \nu^2$ for $\nu < \nu_a$, $F_\nu \propto \nu^{1/3}$ for $\nu_a < \nu < \nu_m$, and $F_\nu \propto \nu^{-(p-1)/2}$ for $\nu > \nu_m$, where p is the electron power-law index. To globally fit the entire radio and optical/IR data set, we employed the smoothed form of the broken

power-law synchrotron spectrum, calculated by Granot et al. (1999a) and Granot et al. (1999b). With this approach, we treat $t_{\rm jet}$, p, and the values of ν_a, ν_m, and $F_{\nu,\rm max}$ at $t = t_{\rm jet}$ as free parameters. This method forces $t_{\rm jet}$ to have the same value at all frequencies. In addition, the shape of the transition from spherical to jet evolution is described by the analytical form $F_\nu = (F^n_{\nu,s} + F^n_{\nu,j})^{1/n}$, with n left as a free parameter. We find the following values for the burst parameters: $t_{\rm jet} = 7.3 \pm 0.5$ days, $p = 2.70 \pm 0.04$, $n = -6$, $\nu_a(t = t_{\rm jet}) = 6.8 \pm 1.8$ GHz, $\nu_m(t = t_{\rm jet}) = (3.3 \pm 0.4) \times 10^{11}$ Hz, and $F_{\nu,\rm max}(t = t_{\rm jet}) = 2.6 \pm 0.2$ mJy, where the errors are the 1σ values derived from the correlation matrix. We note that there is substantial covariance between some of the parameters, and therefore these error estimates should be treated with caution. From our fit, the asymptotic temporal decay slopes of the optical light curves are $\alpha_1 = -3(p-1)/4 = -1.28$ for $t < t_{\rm jet}$, and $\alpha_2 = -p = -2.70$ for $t > t_{\rm jet}$. The fits are shown in Figures 2.1–2.3.

The total value of χ^2 for the global fit is poor. We obtain $\chi^2 = 670$ for 140 degrees of freedom. The bulk of this value, 550, comes from the 102 optical data points, and is the result of the observed fluctuations, which are not accounted for by our model. The radio data contribute a value of 120 to χ^2 for 43 data points. This is the result of scintillation, and the observed late-time flattening of the 8.46 GHz lightcurve. If we increase the errors to accommodate the expected level of scintillation (see §2.3), we obtain a good fit with $\chi^2_{\rm radio} = 45/38$ degrees of freedom.

From Figure 2.1, it is clear that the global fit accurately describes the broad-band spectra on days 4.26 ($t < t_{\rm jet}$) and 12.17 ($t > t_{\rm jet}$), with a single value of $p = 2.70$, which rules out the possibility that the steepening of the lightcurves at $t_{\rm jet}$ is the result of a time-varying p.

Trying to model the data using the approach outlined above, but for a wind-shaped circumburst medium, results in a poor description of the data, because the wind model does not exhibit a break, although one is clearly seen in the optical data. As a result, the model fit is too low at early times, and too high at late times relative to the data (see inset in Figure 2.3). The value of χ^2 for the wind model relative to the ISM+jet model described above is $\chi^2{\rm wind}/\chi^2_{\rm ISM+jet} \approx 4$. Therefore, the wind model can be ruled out as a description of the afterglow of GRB 000301C.

A jet evolution combined with a wind-shaped circumburst medium provides a more reasonable fit than a wind-only model. The wind evolution of the fireball will only be manifested for $t < t_{\rm jet}$, since once $\Gamma(t_{\rm jet}) \approx \theta_0^{-1}$ the jet will expand sideways and appear to observers as if it were expanding into a constant-density medium (Chevalier & Li 1999, 2000; Livio & Waxman 2000; Kumar & Piran 2000). The resulting parameters from such a fit differ considerably from the parameters for the ISM+jet model quoted above, and the relative value of χ^2 between the two models is $\chi^2{\rm wind + jet}/\chi^2_{\rm ISM+jet} \approx 2$. This model suffers from a serious drawback in its description of the optical/IR lightcurves. Because the predicted decay of these lightcurves prior to $t_{\rm jet}$ is steeper than in the ISM+jet model, the model fit, from 2 days after the burst up to the break time, is too low relative to the data (see inset in Figure 2.3).

It is important to note that in a recent paper, Kumar & Piran (2000) suggested that the steepening of the lightcurves when the jet geometry of the outflow becomes manifested is completed over 1 decade in observer time in the case of the ISM+jet scenario, and over $2-4$ decades in observer time in the wind+jet scenario. We can estimate the transition time, δt, by comparing the smooth-transition lightcurves to the asymptotic slopes at times much larger and smaller than $t_{\rm jet}$ (i.e., the same light curves but with a sharp transition). We find that the maximum deviation between the two curves, which occurs at $t_{\rm jet}$, is $\sim 10\%$. If we therefore define the transition time as the period during which the sharp curves deviate by more than 1% (or 5%) from the smooth curves, then we find that the transition time for GRB 000301C is approximately 10 (or 4) days, which gives $\delta t/t_{\rm jet} \approx 1$. This transition time is clearly inconsistent with the extremely gradual steepening in a wind-shaped circumburst medium, but is consistent with the expected transition time in the ISM+jet case. However, Kumar & Piran (2000) claim that the expected change in the power-law index due to the jet break is $\Delta\alpha \sim 0.7$, while the observed steepening in this case is $\Delta\alpha \approx 1.4$. A similar behavior in the afterglow emission from GRB 990510 was explained as the result of the passage of ν_c and ν_m through the optical bands at $t \sim t_{\rm jet}$. In the case of GRB 000301C, however, we expect ν_m to cross the optical band at $t \approx 0.05$ days $\ll t_{\rm jet}$. In the context of this analysis,

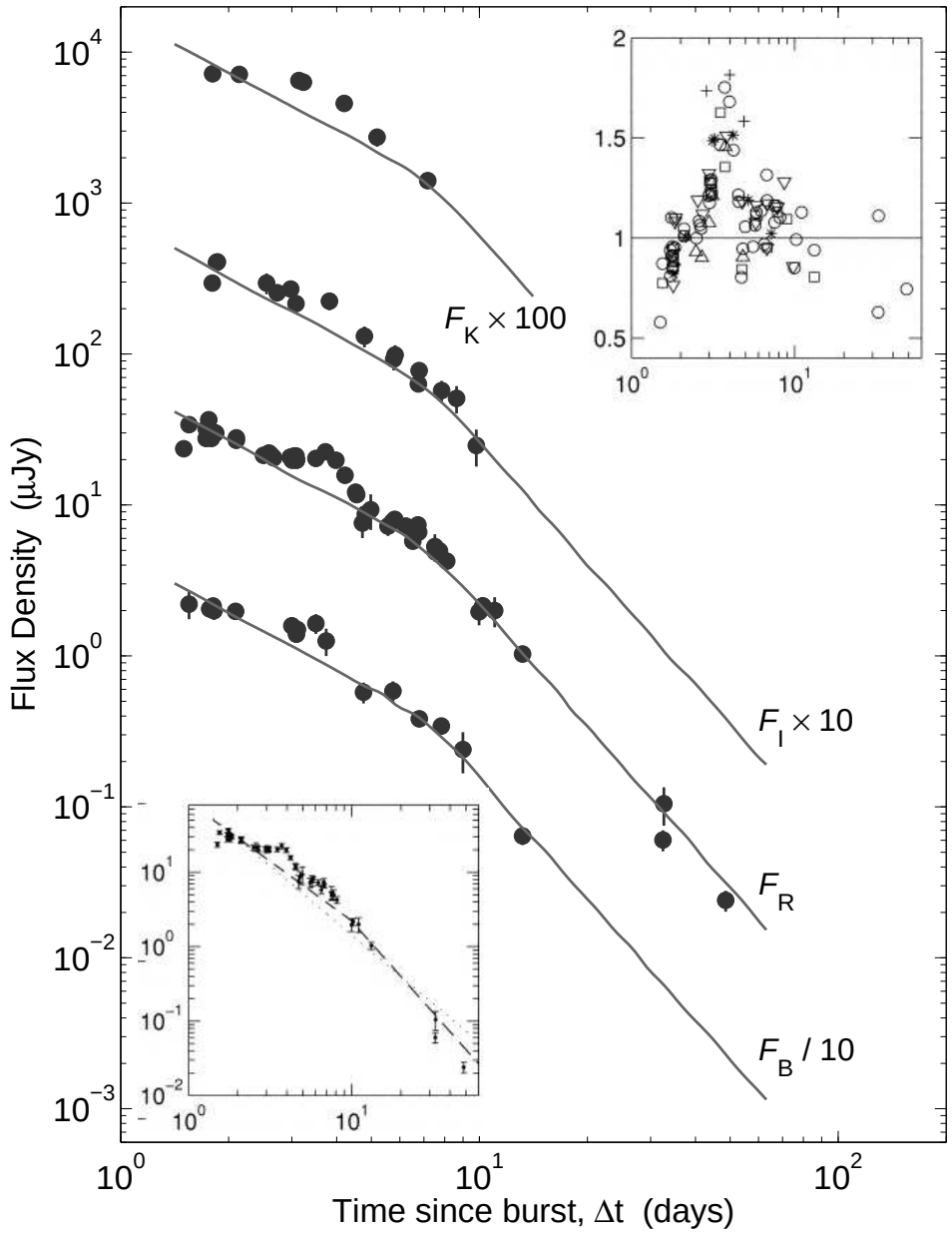

Figure 2.3: Optical/near-IR lightcurves of GRB000301C. Following Masetti et al. (2000a), we added a 5% systematic uncertainty in quadrature to all optical measurements to account for discrepancies between the different telescopes and instruments. The solid lines show the ISM+jet global fit. In the top right inset are plotted the data points divided by the respective model fit for all bands (circles, squares, stars, triangles, inverted triangles, and plus signs: R, B, K', V, I, and 250 GHz bands, respectively). The short-timescale fluctuations are clearly achromatic and with a comparable amplitude in all bands, possibly spanning from optical to radio. The inset in the bottom left portion of the figure shows the global fits based on the wind-only (dotted line), and wind+jet (dashed line) models overlaid on the R-band data. The steeper decline predicted for a fireball expanding into a wind-shaped medium results in a much poorer fit relative to the ISM+jet model (§2.4). Note that the data and fit for the B band were divided by a factor of 10, the data and fit for the I band were multiplied by a factor of 10, and the data and fit for the K' band were multiplied by a factor of 100 to avoid overlap between the four curves.

ν_c does not cross the optical band at all, and in a fit in which ν_c is left as a free parameter, it is expected to cross the optical band at $t \sim 10^{-3}$ days (see §2.5).

The global fitting approach has several advantages over fitting each component of the data set independently. For example, the K' data are only available up to day 7.18 ($\lesssim t_{\rm jet}$) after the burst. Therefore, by fitting them independently of the other optical bands and the radio data, we cannot find $t_{\rm jet}$ if it is indeed after 7 days. Moreover, as we can see from Figure 2.3, there is an additional process that superposes achromatic fluctuations with an overall rise and decline centered between days 3 and 4, on top of the smoothly decaying optical emission (see inset in Figure 2.3), then fitting the K' data independently will confuse this behavior with the jet break. This explains the result of Rhoads & Fruchter (2001) of $t_{\rm jet,K'} \sim 3$ days. It is worth noting that fitting the available R-band data from before day 8 by itself gives a value of $t_{\rm jet,R} \sim 3.5$ days $\sim t_{\rm jet,K'}$.

Simultaneous fitting of the entire data set makes it possible to study the overall behavior of the fireball regardless of any additional sources of fluctuations, because the large range in frequency and time of the data reduces the influence of such fluctuations. Remarkably, using this global fit with only the radio data, ignoring the optical observations, we obtain $t_{\rm jet,radio} \approx 7.7$ days $\sim t_{\rm jet}$. Thus, the radio data serve to support the jet model, and provide an additional estimate for the jet break time, independent of the somewhat ambiguous optical data.

From the global fit, we find the first self-consistent indication that the short-timescale optical fluctuations are achromatic, even in the K' band (see inset in Figure 2.3). By simply dividing the B, V, R, I and K' data by the values from the global fit, we find that the fluctuations happen simultaneously and with similar amplitudes in all bands. Moreover, the overall structure of the fluctuations is a sharp rise and decline centered on day 4, and with an overall width of 3.5 days, which gives $\delta t/t \sim 1$, where δt is the width of the bump. The optical/IR data start at day 1.5 lower by $25-50\%$ than the model fit, then rise to a peak level of $50-75\%$ relative to the model at day 4, and drop to the predicted level at about day 6, at which point they follow the predicted decline of the ISM+jet model.

It is interesting to note that the 250 GHz data, which are not affected by ISS-induced fluctuations, also show a peak amplitude approximately 70% higher than the model fit around day 4 (see Figure 2.2 and inset in Figure 2.3). At the lower radio frequencies, there are not enough data points to discern a similar behavior. Moreover, at these frequencies it would have been difficult to disentangle such fluctuations from ISS-induced fluctuations in any case. The large range in frequency of this achromatic fluctuation, coupled with the similar level of absolute deviation from the model fit, suggests that it is the result of a real physical process.

It is possible to explain this fluctuation as the result of a nonuniform ambient density. The value of ν_m is independent of the ambient medium density, and since $F_{\nu,\rm max} \propto n_1^{1/2}$, we expect the flux at frequencies larger than ν_a to vary achromatically, and with the same amplitude, $F_\nu \propto n_1^{1/2}$. For frequencies lower than ν_a we must take into account the density dependence, $\nu_a \propto n_1^{3/5}$, so that the flux will vary according to $F_\nu \propto F_{\nu,\rm max}\nu_a^{-2} \propto n_1^{-7/10}$. This means that for frequencies lower than ~ 7 GHz, we actually expect the flux to fluctuate downward at the same time that it fluctuates upward at higher frequencies. In practice, we do not have enough data around this time to confirm this behavior, but we do note that the two data points at 8.46 GHz from around day 4 exhibit a lower flux density level than expected from the fit. This discrepancy, however, can also be due to ISS. In order to match the observed peak amplitude of the optical fluctuation, of order 80%, the ambient density must vary by about a factor of 3.

Using the value of $t_{\rm jet}$ from our global fit, we can calculate the jet opening angle, θ_0, from the equation:

$$\theta_0 \approx 0.05 t_{\rm j,hr}^{3/8}(1+z)^{-3/8}(n_1/E_{52})^{1/8} \tag{2.1}$$

(Sari et al. 1999; Livio & Waxman 2000), where E_{52} is the isotropic energy release, which can be roughly estimated from the observed fluence; using the equations from Rhoads (1999) results in a smaller opening angle. From this equation, we calculate a value of $\theta_0 \approx 0.2 n_1^{1/8}$ rad. This means that the actual energy

release from GRB 000301C is reduced by a factor of 50 relative to the isotropic value, $E_{\gamma,\rm iso} \approx 5.4 \times 10^{52}$ erg, which gives $E_\gamma = 1.1 \times 10^{51} n_1^{1/4}$ erg.

SECTION 2.5

Conclusions

The afterglow emission from GRB 000301C can be well described in the framework of the jet model of GRBs. Global fitting of the radio and optical data allows us to calculate the values of p, $t_{\rm jet}$, the time evolution of ν_a, ν_m and $F_{\nu,\rm max}$, and the shape of the transition to jet evolution in a self-consistent manner. Within this approach, the proposed discrepancy between the behaviors of the R- and K'-band lightcurves, suggested by Rhoads & Fruchter (2001), is explained as the result of the lack of data for $t > 7.18$ days ($\lesssim t_{\rm jet}$) at K', and the existence of achromatic substructure from fluctuations in the optical/IR, and possibly the radio regime. The value for the break time from the global, self-consistent approach we have used is $t_{\rm jet} = 7.3$ days at all frequencies.

The long-lived radio emission from the burst, spanning a large range in frequency and time, plays a significant role in our ability to extract the time evolution of ν_a, ν_m and $F_{\nu,\rm max}$ from the data. In the case of this GRB in particular, the large range in frequency and time is crucial, since it serves to reduce the effects of unexplained deviations from the simple theory, such as the short-timescale fluctuations in the optical bands, on the overall evolution of the fireball.

We end with some general remarks about the fit in the case in which ν_c is not constrained to lie above the optical band. If we just add ν_c as an additional free parameter in the fit, we find that the best-fit value for the cooling frequency at $t_{\rm jet}$ is $\nu_c \approx 5 \times 10^{14}$ Hz, while the best-fit values for all other parameters are relatively unchanged (i.e., within 2σ of the values given in §2.4). This value of ν_c indicates that the cooling frequency crosses the optical bands approximately 2 days after the burst. However, the resulting modest steepening of $\Delta\alpha = 1/4$ is overshadowed by the much larger scale overall fluctuation in the optical bands. Using a different approach, in which we fix the value of ν_c and leave all other parameters to vary freely, we find that for all values of ν_c, the value of ν_m is lower than ν_c at $t = t_{\rm jet}$. Finally, we note that in both cases – a fixed or freely varying ν_c – the value of χ^2 is similar to the value for the analysis in §2.4.

Research at the Owens Valley Radio Observatory is supported by the National Science Foundation through NSF grant AST 96-13717. K.H. acknowledges Ulysses support under JPL contract 958056 and NEAR support under NAG5-9503.

Table 2.1. Radio and Submillimeter Observations of GRB 000301C

Epoch (UT)	Δt (days)	Telescope	ν_0 (GHz)	S$\pm\sigma$ (μJy)
2000 Mar 4.29	2.88	IRAM 30-m	250	2100 ± 300
2000 Mar 4.75	3.34	JCMT	350	3736 ± 3700
2000 Mar 4.98	3.57	Ryle	15.0	660 ± 160
2000 Mar 5.41	4.00	IRAM 30-m	250	2300 ± 400
2000 Mar 5.53	4.12	JCMT	350	2660 ± 1480
2000 Mar 5.57	4.16	OVRO	100	2850 ± 950
2000 Mar 5.67	4.26	VLA	1.43	11 ± 79
2000 Mar 5.67	4.26	VLA	4.86	240 ± 53
2000 Mar 5.67	4.26	VLA	8.46	316 ± 41
2000 Mar 5.67	4.26	VLA	22.5	884 ± 216
2000 Mar 6.29	4.88	IRAM 30-m	250	2000 ± 500
2000 Mar 6.39	4.98	VLA	8.46	289 ± 34
2000 Mar 6.50	5.09	JCMT	350	1483 ± 1043
2000 Mar 6.57	5.16	OVRO	100	-99 ± 1500
2000 Mar 9.25	7.84	IRAM 30-m	250	400 ± 600
2000 Mar 10.21	8.80	Ryle	15.0	480 ± 300
2000 Mar 13.58	12.17	VLA	8.46	483 ± 26
2000 Mar 13.58	12.17	VLA	22.5	748 ± 132
2000 Mar 15.58	14.17	VLA	8.46	312 ± 62
2000 Mar 17.61	16.20	VLA	8.46	380 ± 29
2000 Mar 21.52	20.12	VLA	8.46	324 ± 36
2000 Mar 23.55	22.14	VLA	8.46	338 ± 69
2000 Mar 24.29	22.88	IRAM 30-m	250	-300 ± 500
2000 Mar 27.55	26.14	VLA	8.46	281 ± 34
2000 Mar 31.53	30.12	VLA	8.46	281 ± 25
2000 Apr 4.59	34.18	VLA	8.46	325 ± 27
2000 Apr 10.36	39.95	VLA	8.46	227 ± 33
2000 Apr 12.47	42.06	VLA	4.86	210 ± 43
2000 Apr 12.47	42.06	VLA	8.46	91 ± 38
2000 Apr 15.43	45.02	VLA	8.46	233 ± 37
2000 Apr 18.47	48.06	VLA	4.86	226 ± 51
2000 Apr 18.47	48.06	VLA	8.46	145 ± 36
2000 May 4.49	64.13	VLA	4.86	136 ± 45
2000 May 4.49	64.13	VLA	8.46	150 ± 20
2000 May 7.50	67.09	VLA	4.86	85 ± 33
2000 May 7.50	67.09	VLA	8.46	144 ± 31
2000 May 22.45	82.04	VLA	8.46	105 ± 25
2000 May 23.45	83.04	VLA	8.46	114 ± 24
2000 Jun 6.40	96.99	VLA	8.46	110 ± 26
2000 Jun 10.31	100.90	VLA	8.46	96 ± 33
2000 Jun 14.26	104.85	VLA	4.86	45 ± 24
2000 Jun 14.29	104.88	VLA	8.46	77 ± 21
2000 Jul 2.06	122.65	VLA	8.46	48 ± 20

Note. — The columns are (left to right), (1) UT date of the start of each observation, (2) time elapsed since the γ-ray burst, (3) telescope name, (4) observing frequency, and (5) peak flux density at the best fit position of the radio transient, with the error given as the root mean square noise on the image. The JCMT observations did not detect the source at each epoch individually, but by averaging the 3.875 hr of integration over the three epochs, we obtain a 2.5σ detection of 1.70 ± 0.71 mJy.

CHAPTER 3

GRB 000418: A Hidden Jet Revealed†

E. Berger[a], A. Diercks[a], D. A. Frail[b], S. R. Kulkarni[a], J. S. Bloom[a], R. Sari[c], J. Halpern[d], N. Mirabal[d], G. B. Taylor[b], K. Hurley[e], G. Pooley[f], K. M. Becker[g], R. M. Wagner[h], D. M. Terndrup[h], T. Statler[i], D. R. Wik[i], E. Mazets[j], & T. Cline[k]

[a]Department of Astronomy, 105-24 California Institute of Technology, Pasadena, CA 91125

[b]National Radio Astronomy Observatory, P. O. Box 0, Socorro, NM 87801

[c]California Institute of Technology, Theoretical Astrophysics 103-33, Pasadena, CA 91125

[d]Astronomy Department, Columbia University 550 West 120th St., New York, NY 10027

[e]University of California, Berkeley, Space Sciences Laboratory, Berkeley, CA 94720-7450

[f]Mullard Radio Astronomy Observatory, Cavendish Laboratory, Madingley Road, Cambridge CB3 0HE

[g]Department of Physics, Oberlin College Oberlin, OH 44074

[h]Ohio State University, Department of Astronomy, Columbus, OH, 43210

[i]Ohio University, Department of Physics and Astronomy, Athens, OH, 45701

[j]Ioffe Physico-Technical Institute, St. Petersburg, 194021 Russia

[k]NASA Goddard Space Flight Center, Code 661, Greenbelt, MD 20771

Abstract

We report on optical, near-infrared and centimeter radio observations of GRB 000418 which allow us to follow the evolution of the afterglow from 2 to 200 days after the γ-ray burst. In modeling these broad-band data, we find that an isotropic explosion in a constant density medium is unable to simultaneously fit both the radio and optical data. However, a jet-like outflow into either a constant density or wind-stratified medium with an opening angle of 10-20° provides a good description of the data. The evidence in favor of a jet interpretation is based on the behavior of the radio light curves, since the expected jet break is masked at optical wavelengths by the light of the host galaxy. We also find evidence for extinction, presumably arising from within the host galaxy, with A_V^{host}=0.4 mag, and host flux densities of $F_R = 1.1$ μJy and $F_K = 1.7$ μJy. These values supercede previous work on this burst due to the availability of a broad-band data set allowing a global fitting approach. A model in which the GRB explodes isotropically into a wind-stratified circumburst medium cannot be ruled out by these data. However, in examining a sample of other bursts (e.g., GRB 990510, GRB 000301C) we favor the jet interpretation for GRB 000418.

† A version of this chapter was published in *The Astrophysical Journal*, vol. 556, 556-561, (2001).

SECTION 3.1

Introduction

GRB 000418 was detected on 18 April 2000, at 09:53:10 UT by the *Ulysses*, *KONUS-Wind* and *NEAR* spacecraft, which are part of the third interplanetary network (IPN). The event lasted ∼30 s, and a re-analysis of the early Ulysses data (Hurley et al. 2000) gives a fluence of 4.7×10^{-6} erg cm^{-2} in the 25-100 keV band. A fit to the total photon spectrum from the KONUS data in the energy range $15 - 1000$ keV gives a fluence of 2×10^{-5} erg cm^{-2}. Intersecting IPN annuli resulted in a 35 arcmin^2 error box, in which Klose et al. (2000a) identified a variable near-infrared (NIR) source. The early R-band light curve of this source was described by Mirabal et al. (2000) as having a power-law decay $t^{-0.84}$, typical for optical afterglows. The redshift for the host galaxy of $z \simeq 1.119$ was measured by Bloom et al. (2000) from an [OII] emission line doublet. Assuming cosmological parameters of Ω_M=0.3, Λ_0=0.7 and H_0=65 km s^{-1} Mpc^{-1}, this redshift corresponds to a luminosity distance $d_L = 2.5 \times 10^{28}$ cm and gives an implied isotropic γ-ray energy release of $E_\gamma = 1.7 \times 10^{52}$ erg.

Klose et al. (2000b) have recently summarized optical/NIR data observations of GRB 000418. In this paper we present additional optical/NIR data and a complete set of radio observations between 1.4 GHz and 22 GHz, from 10 to 200 days after the burst. We use this broad band data set to fit several models, deriving the physical parameters of the system.

SECTION 3.2

Observations

3.2.1 Optical Observations

In Table 3.1 we present deep optical photometry obtained at Palomar, Keck[1] , and MDM observatories covering six weeks following the GRB as well as data from the extant literature.

All of the optical data was overscan corrected, flat-fielded, and combined in the usual manner using IRAF (Tody 1993). PSF-fitting photometry was performed relative to several local comparison stars measured by Henden (2000) using DoPhot (Schechter et al. 1993). Short exposures of the field in each band were used to transfer the photometry (Henden 2000) to several fainter stars in the field. Several of the Keck+ESI measurements, and the Palomar 200" measurement were made in Gunn-r and Gunn-i respectively and were calibrated by transforming the local comparison stars to the Gunn system using standard transformations (Wade et al. 1979; Jorgensen 1994). We add an additional 5% uncertainty in quadrature with the statistical uncertainties to reflected the inherent imprecision in these transformations.

The Ks-band image of the field was obtained on the Keck I Telescope on Manua Kea, Hawaii with the Near Infrared Camera (NIRC; Matthews & Soifer 1994). We obtained a total of 63 one-minute exposures which we reduced and combined with the `IRAF/DIMSUM` package modified by D. Kaplan. There was significant cloud and cirrus cover and so the night was not photometric.

The HST STIS/Clear image was obtained on 4 June 2000 UT as part of the TOO program # 8189 (P.I. A. Fruchter) and made public on 2 September 2000 UT. Five images of 500 s each were obtained which we combined using the `IRAF/DITHER` task. The final plate scale is 25 milliarcsec pixel^{-1}.

We corrected all optical measurements in Table 3.1 for a Galactic foreground reddening of $E(B-V) = 0.032$ (Schlegel et al. 1998) at the position of the burst $(l, b) = (261.16, 80.78)$ before converting to flux units Bessell & Brett (1988); Fukugita et al. (1995) assuming R_V=3.1.

[1] The W. M. Keck Observatory is operated by the California Association for Research in Astronomy, a scientific partnership among California Institute of Technology, the University of California and the National Aeronautics and Space Administration.

3.2.2 Radio Observations

Radio observations were undertaken at a frequency of 15 GHz with the Ryle Telescope. All other frequencies were observed with either the NRAO[2] Very Large Array (VLA) or the Very Long Baseline Array (VLBA). A log of these observations can be found in Table 3.2. The data acquisition and calibration for the Ryle and the VLA were straightforward (see Frail et al. 2000a for details).

The single VLBA observation was carried out at 8.35 GHz with a total bandwidth of 64 MHz in a single polarization using 2 bit sampling for additional sensitivity. The nearby ($<1.3^\circ$) calibrator J1224+2122 was observed every 3 minutes for delay, rate and phase calibration. Amplitude calibration was obtained by measurements of the system temperature in the standard way. The coordinates for GRB 000418 derived from the VLBA detection are (epoch J2000) $\alpha = 12^h25^m19.2840^s$ ($\pm 0.015^s$) $\delta = +20^\circ06'11.141''$ ($\pm 0.001''$).

SECTION 3.3

The Optical Light Curve and Host Galaxy

In Figure 3.1 we display the R and K-band light curves constructed from measurements in Table 3.1. The pronounced flattening of the R-band light curve at late times is reasonably attributed to the optical afterglow fading below the brightness of the underlying host galaxy. A noise-weighted least squares fit was made to the data of the form $f_R = f_o t_o^\alpha + f_{host}$ for which we derive $f_o = 23.4 \pm 2.1$ μJy, $\alpha_o = -1.41 \pm 0.08$ and $f_{host} = 1.08 \pm 0.06$ μJy with a reduced $\chi^2_r = 0.94$. Our inferred R-band magnitude for the host galaxy $R_{host} = 23.66 \pm 0.06$ is nearly identical to that obtained from a similar analysis by Klose et al. (2000b). In order to estimate the effect of the host in other optical bands we scaled R_{host} for GRB 000418 to a spectrum of the host galaxy of GRB 980703 (Bloom et al. (1998a)) ($z = 0.966$) whose magnitude was measured in seven broad-band colors (B, V, R, I, J, H, and K). Our results indicate that 50-100% of the flux in some bands is due to the host galaxy after the first 10 days. Therefore, for the afterglow modeling in §3.5 we chose not to include the late-time measurements of GRB 000418 in the B, V, and Gunn-i bands.

SECTION 3.4

The Radio Light Curves

In Figure 3.1 we display the radio light curves at 4.86, 8.46, 15 and 22 GHz. To first order all four frequencies show a maximum near 1 mJy on a time scale of 10 to 20 days. There is no discernible rising trend at any frequency. This is most clear at 8.46 GHz, where beginning 10 days after the burst, the light curve undergoes a steady decline, fading from 1 mJy to 0.1 mJy over a six month period. The temporal slope of the 8.46 GHz light curve after the first two months $\alpha_{\rm rad} = -1.37 \pm 0.10$ ($\chi^2_r = 1.4$) is similar to the optical R-band curve $\alpha_{\rm opt} = -1.41 \pm 0.08$.

Superimposed on this secular decrease, there exists point-to-point variability of order 50%, especially in the early measurements. We attribute these variations to interstellar scintillation (ISS). The method by which we estimate the magnitude of the intensity fluctuations induced by ISS as a function of frequency and time is described in full by Berger et al. (2000). Briefly, we estimate the magnitude of scattering with the model of Taylor & Cordes (1993), and use this to calculate the transition frequency ν_0 between weak and strong scattering using Walker 1998. The normalizations used in Goodman (1997) give slightly larger values of ν_0.

In the direction toward GRB 000418 we derive $\nu_0 \simeq 3.6$ GHz and therefore most of our measurements were taken in the weak ISS regime. In this case the modulation scales as $\nu^{-17/12}$, with a maximum of 65% expected at 4.86 GHz and 30% at 8.46 GHz. At 15 GHz and 22 GHz we estimate that the

[2] The NRAO is a facility of the National Science Foundation operated under cooperative agreement by Associated Universities, Inc. NRAO operates the VLA and the VLBA

ISS-induced fluctuations are only a fraction of the instrumental noise. The expansion of the fireball will eventually quench ISS when the angular size of the fireball exceeds the angular size of the first Fresnel zone at the distance of the scattering screen. The fireball size, and hence the quenching timescale, is model-dependent, and we use the derived total energy and density from the global fits (see §3.5 below) to estimate this time for each model. For example, in a simple spherical fireball this occurs after 15 days at 4.86 GHz and 10 days at 8.46 GHz, and thereafter the modulation indices decline as $t^{-35/48}$. We note that the observed fluctuations at 4.86 and 8.46 GHz conform to the predicted level of ISS, but that the measurements at 8.46 GHz from around 50 days after the burst deviate by a factor of three from the predicted ISS level.

In addition, we use the scintillation pattern to estimate the true χ^2_r for each model, by adding in quadrature to the instrumental noise an additional ISS-induced uncertainty, $\sigma_{\rm ISS} = m_p F_{\nu,{\rm model}}$, where m_p and $F_{\nu,{\rm model}}$ are the modulation index and model flux density at frequency ν, respectively (Berger et al. 2000).

SECTION 3.5

Global Model Fits

The optical and radio data presented here have allowed us to track the evolution of the GRB 000418 afterglow from 2 to 200 days after the burst. With careful modeling of the light curves, it should be possible to infer the physical parameters of the blast wave and thereby gain some insight into the nature of GRB progenitors. In particular, the hydrodynamic evolution of the shock is governed by the energy of the explosion, the geometry of the expanding ejecta shock and the type of environment into which the GRB explodes (Sari et al. 1998; Wijers & Galama 1999; Chevalier & Li 1999; Panaitescu & Kumar 2000). We consider four basic models: a spherical explosion or collimated ejecta (i.e., jets) in both a constant density medium and a wind-blown medium.

The starting point for any afterglow interpretation is the cosmological fireball model (e.g., Meszaros & Rees 1997; Waxman 1997). A point explosion of energy E_0 expands relativistically into the surrounding medium (with density $\rho \propto r^{-s}$, where $s = 0$ for constant density ISM and $s = 2$ for a wind) and the shock produced as a result of this interaction is a site for particle acceleration. The distribution of electrons is assumed to be a power-law of index p, and the fraction of the shock energy available for the electrons and the magnetic field is ϵ_e and ϵ_B, respectively. The values of these three quantities (p, ϵ_e and ϵ_B) are determined by the physics of the shock and the process of particle acceleration and in the absence of detailed understanding are taken to be constant with time.

The instantaneous broad-band synchrotron spectrum can be uniquely specified by the three characteristic frequencies ν_a, ν_m, and ν_c, (i.e., synchrotron self-absorption, synchrotron peak, and cooling), the peak flux density f_m, and p. For this work we adopt the smooth spectral shape as given by Granot et al. (1999a), rather than the piecewise, broken power-law spectrum used by other authors (e.g., Wijers & Galama 1999). The evolution of the spectrum (and thus the time dependence of ν_a, ν_m, ν_c and f_m) is governed by the geometry of the explosion (spherical or a collimated into a jet-like outflow), and the properties of the external environment (constant density or a radial density profile). Our approach is to adopt a model (sphere, wind, jet, etc.) and solve for the above spectral parameters using the entire optical and radio data set. The advantages and details of global model fitting are discussed by Berger et al. (2000).

The simplest model is a spherically symmetric explosion in a constant density medium (*ISM*: Sari et al. 1998). The total χ^2_r for this model (see Table 3.3) gives a highly unsatisfactory fit to the data. On close inspection (Figure 3.1) we find that the model systematically underpredicts the optical flux. Adding extinction from the host galaxy only makes this worse. The fundamental difficulty with the *ISM* model is that it predicts $f_m = constant$, independent of frequency. In this case, since it is the radio data that is responsible for defining the peak of spectrum, it results in a value of f_m that is too low at higher frequencies.

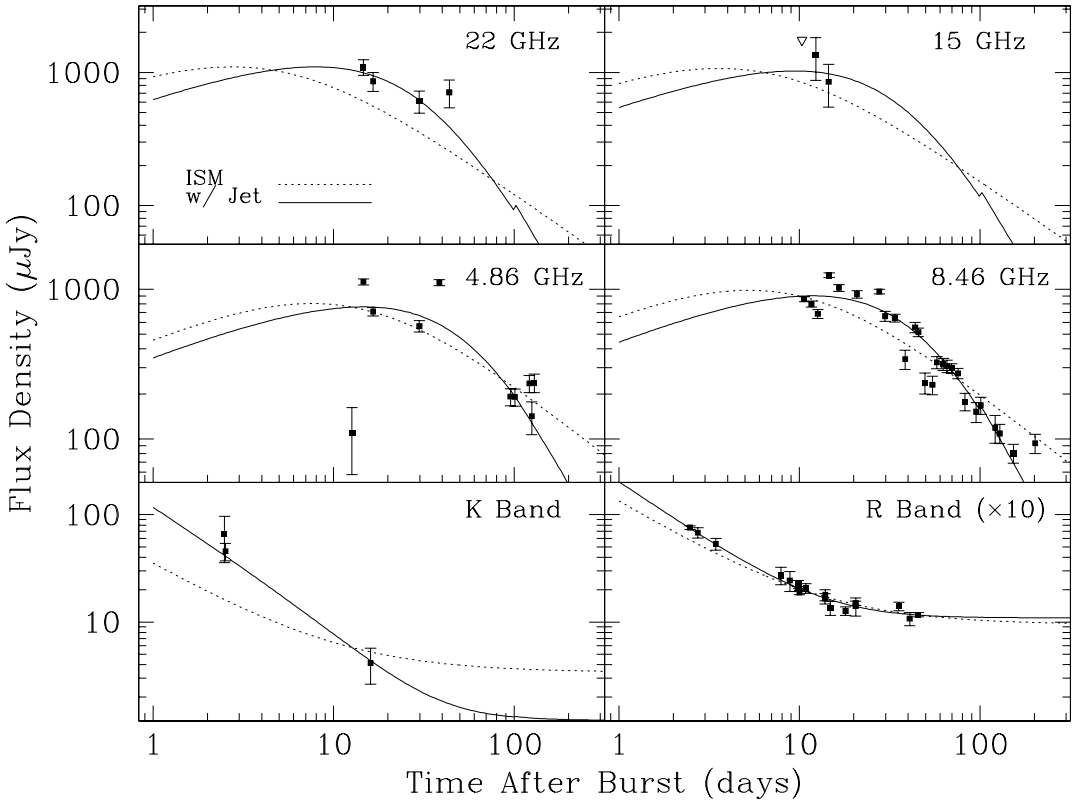

Figure 3.1: Radio and optical light curves for GRB 000418. The observing frequency (or band) is shown in the upper right corner of each panel. Optical magnitudes were first corrected for Galactic forground reddening before converting to flux units. For display purposes the R band flux densities have been increased by a factor of 10. The 8.46 GHz measurements on August 25 and September 18 are 3-epoch averages taken over a period of 7 days and 15 days, respectively. The dotted and solid lines are light curves assuming an isotropic explosion in a constant density medium (ISM) and one in which the ejecta are collimated with opening angle θ_j (ISM+Jet), respectively. They were derived from a global fit to the entire broad-band dataset. See text for more details.

To obtain better fits to the joint optical and radio data sets we look to models for which f_m is time-dependent. One such model is a collimated outflow into a medium with uniform density (*ISM+Jet*: Rhoads 1997, 1999; Sari et al. 1999). The clearest observational signature of a jet is an achromatic break in the light curves at t_j (e.g., Harrison et al. 1999). At radio wavelengths (i.e., below ν_m) at t_j we expect a transition from a rising $t^{1/2}$ light curve to a shallow decay of $t^{-1/3}$, while at optical wavelengths the decay is expected to steepen to t^{-p}. These decay indices refer to the asymptotic values.

Detecting a jet transition at optical wavelengths may be difficult if it occurs on timescales of a week or more. In these cases the afterglow is weak and the light from the host galaxy may start to dominate the light curve (e.g., Halpern et al. 2000). In such instances radio observations may be required to clarify matters, since the radio flux is increasing prior to t_j and changes in the light curve evolution due to the jet break are easily detected. Indeed, the jet in GRB 970508, which was very well observed in the radio is not discernible in the optical data. In this case, Frail et al. (2000c) found a wide-angle jet with an opening angle of 30° and $t_j \sim 30$ days (but see Chevalier & Li 2000).

A *ISM+Jet* model with $t_j \approx 26$ days fits the data remarkably well (see Figure 3.1). The strongest point in favor of this model is that it reproduces the broad maximum (∼1 mJy) seen from 5 GHz to 22 GHz. We expect such a plateau at t_j as all light curves for $\nu_a < \nu \leq \nu_m$ reach their peak fluxes (with only a weak $\nu^{1/3}$ frequency dependence) before undergoing a slow decline. Most other models predict a

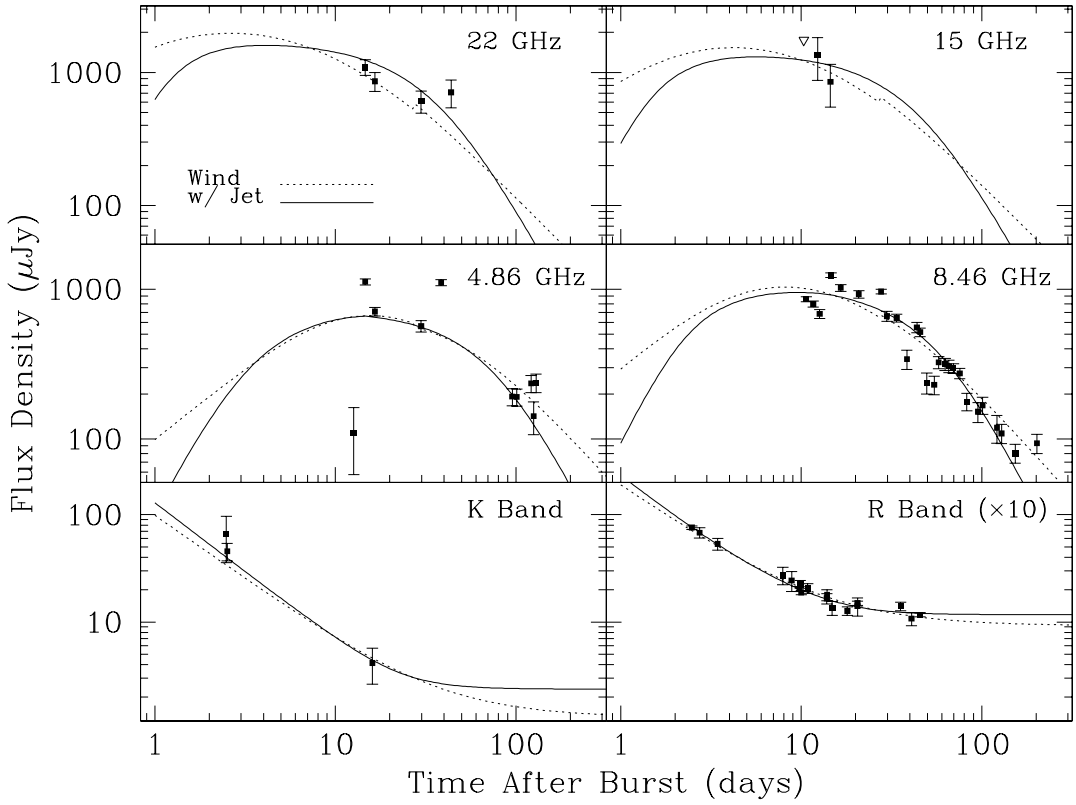

Figure 3.2: Similar to Figure 3.1 but the dotted and solid lines are light curves assuming an isotropic explosion in a wind-blown circumburst medium (Wind) and one in which the ejecta are collimated with opening angle θ_j (Wind+Jet), respectively.

strong frequency dependence in peak flux which is not seen in this case.

Knowing t_j and the density of the ambient medium n_0 from the model fit (Table 3.3) we can make a geometric correction to the total isotropic energy E_γ, as determined from either the observed γ-ray fluence or the total energy of the afterglow E_{52}, from the fit to the afterglow data. This approach gives values for the jet opening angle θ_j between 10° and 20°, which for a two-sided jet reduces the GRB energy to $\sim 10^{51}$ erg. The rapid lateral expansion of the jet also accelerates the transition to the non-relativistic regime, resulting in a change in the evolution of the light curves. Since this occurs on a timescale $t_{\rm NR} \sim t_j \theta_j^{-2} \sim 350$ days (Waxman et al. 1998), we do not expect the non-relativistic transition to be important for our data.

There is some freedom in our choice of ν_c. We know that a cooling break (i.e., $\Delta\alpha = -0.25$) is not apparent in the R band light curve on timescales of 2-10 days, so we searched for solutions with ν_c above or below this frequency. We found that physically consistent solutions (i.e., with non-negative host fluxes, and $\epsilon_B < 1$) were only possible for values of ν_c below the optical band.

As part of the fitting process we also solved for the host flux density in the R and K bands and for any local dust obscuration, assuming an LMC-like extinction law. This yields f_{host}(R)=1.1 μJy, f_{host}(K)=1.7 μJy and A_V^{host}=0.4 (in the host galaxy restframe). Klose et al. (2000b) argued for significant dust extinction with A_V^{host}=0.96. However, they likely overestimated A_V^{host} since they assumed a spherical fireball model and arbitrarily located ν_c above the optical band. Moreover, we find that there is some covariance between the values of A_V^{host} and p so that only with a global fit, in which p is constrained by the radio data as well as the optical data, we can solve for A_V^{host} in a self-consistent manner.

In view of the claims linking GRBs with the collapse of massive stars (Galama et al. 1998a; Bloom

et al. 1999; Reichart 1999; Piro et al. 2000), we consider models of either spherical or jet-like explosions into a wind-blown circumburst medium (*Wind*: Chevalier & Li 1999; Li & Chevalier 1999). The wind models (Figure 3.2) fit the data as well as the *ISM+Jet* model. In fact the χ^2 is lowest for the *Wind + Jet* model. However, in view of the uncertainties in estimating the contribution of ISS to the radio flux variations (§3.4), we do not consider these differences as significant. The close match between the temporal slopes of the late-time 8.46 GHz light curve and the early R band light curve (see §3.4) is a point in favor of the *Wind* model since a steeper decline is expected for a jet geometry. Our failure to distinguish between different models of the circumburst medium can be attributed to the absence of radio measurements (particularly at millimeter wavelengths) at early times. The rapid rise of the flux density below ν_a and ν_m in the *Wind* model and the strong frequency dependence of the peak flux (see Figure 3.1), make such measurements advantageous. Moreover, in principle the *Wind* model can be distinguished from the other models by the fact that in this model ν_c is increasing with time ($\nu_c \propto t^{1/2}$). However, in this case since ν_c lies below the optical/IR bands, this behavior would be distinguishable only at late time when the host flux dominates over the OT. As before we solved for the host flux and any dust extinction (see Table 3.3).

In summary, we find that the radio and optical/NIR observations of the afterglow emission from GRB 000418 can be fit by two different models. The close similarity between the results of the *Wind* and *Jet* models has been noted for other GRBs: 970508 (Frail et al. 2000c; Chevalier & Li 2000), 980519 (Frail et al. 2000b; Chevalier & Li 1999; Jaunsen et al. 2001), 000301C (Berger et al. 2000; Li & Chevalier 2001), and 991208 (Galama et al. 2000; Li & Chevalier 2001). The resolution of this conflict is important, since it goes to the core of the GRB progenitor issue. If the GRB progenitor is a massive star then there must be evidence for a density gradient in the afterglow light curves, reflecting the stellar mass loss that occurs throughout the star's lifetime (Chevalier & Li 1999; Panaitescu & Kumar 2000). At present, an unambiguous case for a GRB afterglow expanding into a wind has yet to be found. On the contrary, most afterglows are better fit by a jet expanding in a constant density medium (e.g., Harrison et al. 1999; Halpern et al. 2000; Panaitescu & Kumar 2000) and thus we are faced with a peculiar situation. While there is good evidence linking GRBs to the dusty, gas-rich environments favored by hypernova progenitors (Bloom et al. 2002a; Galama & Wijers 2001), the expected mass loss signature is absent (or at best ambiguous) in all afterglows studied to date.

AD is supported by a Millikan Fellowship at Caltech. GRB research at Caltech is supported by NSF and NASA grants (SRK, SGD, FAH). KH is grateful for Ulysses support under JPL Contract 958056, and for NEAR support under NAG 5 9503.

Table 3.1. Optical/Near-IR Observations of GRB 000418

UT Date	Instr.[a]	Band	Mag.[b]	Err.	Ref.[c]
Apr 20.89	TNG 3.5m	R	21.54	0.04	2
Apr 20.90	CA 3.5m	K′	17.49	0.5	2
Apr 20.93	CA 1.2m	K′	17.89	0.2	2
Apr 21.15	MDM 2.4m	R	21.66	0.12	1
Apr 21.86	LO 1.5m	R	21.92	0.14	2
Apr 26.316	USNO 1.3m	R	22.65	0.20	2,4
Apr 27.26	MDM	R	22.77	0.23	1
Apr 28.170	P200	R	22.97	0.06	1
Apr 28.3	MDM	R	22.86	0.09	1
Apr 28.413	Keck/ESI	R	23.05	0.05	1
Apr 29.26	MDM	R	22.95	0.11	1
May 2.274	Keck/ESI	Gunn-i	23.38	0.05	1
May 2.28	MDM	R	23.19	0.12	1
May 2.285	Keck/ESI	B	24.31	0.08	1
May 2.31	USNO 1.3m	R	23.11	0.130	2
May 3.26	USNO 1.3m	R	23.41	0.160	2
May 4.44	UKIRT 3.8m	K	20.49	0.40	2
May 6.42	Keck/LRIS	R	23.48	0.10	7
May 8.89	TNG	R	23.30	0.05	2
May 8.92	TNG	V	23.92	0.07	2
May 9.82	USNO 1.0m	R	23.37	0.21	2
May 23.93	TNG	R	23.37	0.10	2
May 29.228	P200	R	23.66	0.15	1
Jun 2.88	CA 3.5m	R	23.32	0.08	2
Jun 2.91	TNG	R	23.57	0.05	2

[a]CA 3.5m=Calar Alto 3.5-meter, USNO1.3m=U.S. Naval Observatory Flagstaff Station 1.3-meter, ESI=W.M. Keck Observatory Echellette Spectrograph-Imager, LRIS=W.M. Keck Observatory Low-Resolution Imaging Spectrograph

[b]Optical photometry is on the Kron-Cousins and Gunn systems and referred to that of Henden (2000). Data are corrected for Galactic extinction corresponding to $E(B-V) = 0.032$ derived from the maps of Schlegel et al. (1998).

[c]1=this work, 2=Klose et al. (2000b), 3=Henden et al. (2000), 4=Metzger & Fruchter (2000)

Table 3.2. Radio Observations of GRB 000418

Epoch (UT)	Telescope	ν_0 (GHz)	S$\pm\sigma$ (μJy)	Epoch (UT)	Telescope	ν_0 (GHz)	S$\pm\sigma$ (μJy)
2000 Apr 28.75	Ryle	15.0	550±600	2000 Jun 3.04	VLA	8.46	517±34
2000 Apr 29.07	VLA	8.46	856±33	2000 Jun 7.01	VLA	8.46	238±38
2000 Apr 30.07	VLA	8.46	795±37	2000 Jun 11.93	VLA	8.46	230±33
2000 Apr 30.73	Ryle	15.0	1350±480	2000 Jun 15.13	VLA	8.46	325±30
2000 May 1.06	VLA	4.86	110±52	2000 Jun 20.10	VLA	8.46	316±30
2000 May 1.06	VLA	8.46	684±48	2000 Jun 23.19	VLA	8.46	306±29
2000 May 2.93	Ryle	15.0	850±300	2000 Jun 27.08	VLA	8.46	296±22
2000 May 3.04	VLA	4.86	1120±52	2000 Jul 2.98	VLA	8.46	274±22
2000 May 3.04	VLA	8.46	1240±46	2000 Jul 10.04	VLA	8.46	178±24
2000 May 3.04	VLA	22.46	1100±150	2000 Jul 22.81	VLA	8.46	152±23
2000 May 4.97	VLA	1.43	210±180	2000 Jul 22.81	VLA	4.86	192±25
2000 May 4.97	VLA	4.86	710±47	2000 Jul 28.50	VLA	8.46	168±22
2000 May 4.97	VLA	8.46	1020±53	2000 Jul 28.50	VLA	4.86	191±25
2000 May 4.97	VLA	22.46	860±141	2000 Aug 17.74	VLA	8.46	119±25
2000 May 7.18	VLBA	8.35	625±60	2000 Aug 17.74	VLA	4.86	235±31
2000 May 9.25	VLA	8.46	926±53	2000 Aug 21.65	VLA	4.86	142±35
2000 May 16.13	VLA	8.46	963±34	2000 Aug 21.65	VLA	8.46	87±31
2000 May 18.24	VLA	4.86	567±50	2000 Aug 25.78	VLA	4.86	238±34
2000 May 18.24	VLA	8.46	660±50	2000 Aug 25.78	VLA	8.46	166±27
2000 May 18.24	VLA	22.46	610±114	2000 Aug 27.89	VLA	8.46	100±25
2000 May 22.21	VLA	8.46	643±38	2000 Sep 10.73	VLA	8.46	148±25
2000 May 26.92	VLA	4.86	1105±51	2000 Sep 18.68	VLA	8.46	55±20
2000 May 26.92	VLA	8.46	341±50	2000 Sep 26.62	VLA	8.46	85±22
2000 Jun 1.14	VLA	8.46	556±43	2000 Nov 6.55	VLA	8.46	94±14
2000 Jun 1.14	VLA	22.46	710±16				

Note. — The columns are (left to right), (1) UT date of the start of each observation, (2) telescope name, (3) observing frequency, and (4) peak flux density at the best fit position of the radio transient, with the error given as the root mean square noise on the image.

Table 3.3. Synchrotron Model Parameters for GRB 000418

Parameters[a]	ISM	ISM+Jet	Wind	Wind+Jet
ν_a (Hz)	4.1×10^9	1.7×10^9	30×10^9	3.7×10^9
ν_m (Hz)	2.3×10^{11}	1.8×10^{10}	5.8×10^{11}	1.1×10^{11}
ν_c (Hz)	2×10^{15}	10^{14}	1.8×10^{13}	5×10^{12}
f_m (mJy)	2.5	3.4	10.4	3.7
p	2.3	2.4	2.2	2.5
t_j (days)	···	25.7	···	14.6
A_V^{host}	0.0	0.4	0.3	0.2
χ^2/dof	326/54	165/53	184/53	127/53
E_{52}	11	10	4	1.6
n_0 or A^*	0.01	0.02	0.14	0.07
ϵ_B	0.05	0.06	0.04	0.70
ϵ_e	0.03	0.10	0.07	0.14

[a]For the *ISM* and *Wind* models ν_a, ν_m, ν_c and f_m are the self-absorption, synchrotron peak, and cooling frequencies, and the peak flux density, respectively on day 1. For the *ISM+Jet* and *Wind+Jet* model these values are referenced instead to the jet break time t_j. p is the electron power-law index and A_V is the V band extinction in the rest frame of the host galaxy (z=1.118), assuming an LMC-like extinction curve. The resulting values of χ^2 include an estimated contribution of interstellar scattering (ISS) and the increased error in subtracting off a host galaxy flux from each of the optical points. The model parameters are the total isotropic energy E_{52} in units of 10^{52} erg, the ambient density n_0 in cm^{-3} or in the case of the two wind models the parameter A^* as defined by Chevalier & Li (1999). ϵ_e and ϵ_B are the fraction of the shock energy in the electrons and the magnetic field, respectively. The true uncertainties in the derived parameters are difficult to quantify due to covariance, but we estimate that they range from $10-20\%$

CHAPTER 4

A Standard Kinetic Energy Reservoir in Gamma-Ray Burst Afterglows†

E. Berger[a], S. R. Kulkarni[a], & D. A. Frail[b]

[a]Department of Astronomy, 105-24 California Institute of Technology, Pasadena, CA 91125, USA

[b]National Radio Astronomy Observatory, P. O. Box 0, Socorro, NM 87801

Abstract

We present a comprehensive sample of X-ray observations of 41 γ-ray burst (GRB) afterglows, as well as jet opening angles, θ_j for a subset with measured jet breaks. We show that there is a significant dispersion in the X-ray fluxes, and hence isotropic X-ray luminosities ($L_{X,\rm iso}$), normalized to $t = 10$ hr. However, there is a strong correlation between $L_{X,\rm iso}$ and the beaming fractions, $f_b \equiv [1 - \cos(\theta_j)]$. As a result, the true X-ray luminosity of GRB afterglows, $L_X = f_b L_{X,\rm iso}$, is approximately constant, with a dispersion of only a factor of two. Since $\epsilon_e E_b \propto L_X$, the strong clustering of L_X directly implies that the adiabatic blastwave kinetic energy in the afterglow phase, E_b, is tightly clustered. The narrow distribution of L_X also suggests that $p \approx 2$, that inverse Compton emission does not in general dominate the observed X-ray luminosity, and that radiative losses at $t < 10$ hr are relatively small. Thus, despite the large diversity in the observed properties of GRBs and their afterglows the energy imparted by the GRB central engine to the relativistic ejecta is approximately constant.

SECTION 4.1

Introduction

Gamma-ray bursts (GRBs) exhibit a remarkable diversity: Fluences range from 10^{-7} to 10^{-3} erg cm^{-2}, peak energies range from 50 keV to an MeV, and possibly from the X-ray to the GeV band (Fishman & Meegan 1995), and durations extend from about 2 to 10^3 s (for the long-duration GRBs). This diversity presumably reflects a dispersion in the progenitors and the properties of the central engine. Perhaps the most impressive feature of GRBs are their brilliant luminosities and isotropic energy releases approaching the rest mass of a neutron star, $E_{\gamma,\rm iso} \sim 10^{54}$ erg (Kulkarni et al. 1999a; Andersen et al. 2000).

The quantity of energy imparted to the relativistic ejecta, $E_{\rm rel}$, and the quality parameterized by the bulk Lorentz factor, Γ, are the two fundamental properties of GRB explosions. In particular, extremely

† A version of this chapter was published in *The Astrophysical Journal*, vol. 590, 379–385, (2003).

high energies push the boundaries of current progenitor and engine models, while low energies could point to a population of sources that is intermediate between GRBs and core-collapse supernovae.

The true energy release depends sensitively on the geometry of the ejecta. If GRB explosions are conical (as opposed to spherical) then the true energy release is significantly below that inferred by assuming isotropy. Starting with GRB 970508 (Waxman et al. 1998; Rhoads 1999) there has been growing observational evidence for collimated outflows, coming mainly from achromatic breaks in the afterglow light curves.

In the conventional interpretation, the epoch at which the afterglow light curves steepen ("break") corresponds to the time at which Γ decreases below θ_j^{-1}, the inverse opening angle of the collimated outflow or "jet" (Rhoads 1999). The break happens for two reasons: an edge effect, and lateral spreading of the jet which results in a significant increase of the swept up mass. Many afterglows have $t_j \sim 1-$few days, which are best measured from optical/near-IR light curves (e.g., Harrison et al. 1999; Kulkarni et al. 1999a; Stanek et al. 1999), while wider opening angles are easily measured from radio light curves (e.g., Waxman et al. 1998; Berger et al. 2001a).

Recently, Frail et al. (2001) inferred θ_j for fifteen GRB afterglows from measurements of t_j and found the surprising result that $E_{\gamma,\rm iso}$ is strongly correlated with the beaming factor, f_b^{-1}; here, $f_b \equiv [1-\cos(\theta_j)]$ is the beaming fraction and $E_{\gamma,\rm iso}$ is the γ-ray energy release inferred by assuming isotropy. In effect, the true γ-ray energy release, $E_\gamma = f_b E_{\gamma,\rm iso}$ is approximately the same for all the GRBs in their sample, with a value of about 5×10^{50} erg (assuming a constant circumburst density, $n_0 = 0.1$ cm^{-3}). In the same vein, broad-band modeling of several GRB afterglows indicates that the typical blastwave kinetic energy in the adiabatic afterglow phase is $E_b \sim 5 \times 10^{50}$ erg, with a spread of about 1.5 orders of magnitude (Panaitescu & Kumar 2002). However, the general lack of high quality afterglow data severely limits the application of the broad-band modeling method.

Separately, Kumar (2000) and Freedman & Waxman (2001) noted that the afterglow flux at frequencies above the synchrotron cooling frequency, ν_c, is proportional to $\epsilon_e dE_b/d\Omega$, where ϵ_e is the fraction of the shock energy carried by electrons and $dE_b/d\Omega$ is the energy of the blastwave per unit solid angle. The principal attraction is that the flux above ν_c does not depend on the circumburst density, and depends only weakly on the fraction of shock energy in magnetic fields, ϵ_B. For reasonable conditions (which have been verified by broad-band afterglow modeling, e.g., Panaitescu & Kumar 2002), the X-ray band ($2-10$ keV) lies above ν_c starting a few hours after the burst. Thus, this technique offers a significant observational advantage, namely the X-ray luminosity can be used as a surrogate for the isotropic-equivalent afterglow kinetic energy.

Piran et al. (2001) find that the X-ray flux, estimated at a common epoch ($t = 11$ hr), exhibits a narrow distribution of $\log(F_X)$, $\sigma_l(F_X) = 0.43^{+0.12}_{-0.11}$; here $\sigma_l^2(x)$ is the variance of $\log(x)$. Taken at face value, the narrow distribution of F_X implies a narrow distribution of $\epsilon_e dE_b/d\Omega$. This result, if true, is quite surprising since if the result of Frail et al. (2001) is accepted then $dE_b/d\Omega$ should show a wide dispersion comparable to that of f_b^{-1}.

Still, Piran et al. (2001) extend their statistical analysis with the following argument. The relation between $dE_b/d\Omega$ and E_b can be restated as $\log(dE_b/d\Omega) = \log(E_b) + \log(f_b^{-1})$. Thus, $\sigma_l^2(dE_b/d\Omega) = \sigma_l^2(E_b) + \sigma_l^2(f_b^{-1})$. Since $dE_b/d\Omega \propto L_{X,\rm iso}$ (for a constant ϵ_e) they express, $\sigma_l^2(E_b) = \sigma_l^2(L_{X,\rm iso}) - \sigma_l^2(f_b^{-1})$. Given the diversity in θ_j (Frail et al. 2001) and the apparent narrowness in F_X (above), it would then follow that E_b should be very tightly clustered.

However, the approach of Piran et al. (2001) makes a key assumption, namely that E_b and f_b^{-1} are uncorrelated. This is certainly true when E_b is constant, but the assumption then pre-supposes the answer! In reality, a correlation between E_b and f_b can either increase or decrease $\sigma_l^2(E_b)$, and this must be addressed directly. In addition, as appears to be the case (see §4.2), $\sigma_l^2(f_b^{-1})$ is dominated by bursts with the smallest opening angles, which results in a distinctly different value than the one used by Piran et al. (2001) based only on the observed values of θ_j.

In this paper, we avoid these concerns by taking a direct approach: we measure the variance in $E_b \propto f_b L_{X,\rm iso}$ rather than bounding it through a statistical relation. We show, with a larger sample,

that $L_{X,\rm iso}$ is not as narrowly distributed as claimed by Piran et al. (2001), and in fact shows a spread similar to that of $E_{\gamma,\rm iso}$. On the other hand, we find that $L_{X,\rm iso}$ is strongly correlated with f_b^{-1}. It is this correlation, and not the claimed clustering of $L_{X,\rm iso}$, that results in, and provides a physical basis for the strong clustering of L_X and hence the blastwave kinetic energy, E_b.

SECTION 4.2

X-ray Data

In Table 4.1 we provide a comprehensive list of X-ray observations for 41 GRB afterglows, as well as temporal decay indices, α_X ($F_\nu \propto t^{\alpha_X}$), when available. In addition, for a subset of the afterglows for which jet breaks have been measured from the radio, optical, and/or X-ray emission, we also include the inferred θ_j (Frail et al. 2001; Panaitescu & Kumar 2002). We calculate θ_j from t_j using the circumburst densities inferred from broad-band modeling, when available, or a fiducial value of 10 cm^{-3}, as indicated by the best-studied afterglows (e.g., Yost et al. 2002). This normalization for n_0 is different from Frail et al. (2001) who used $n_0 = 0.1$ cm^{-3}.

For all but one burst we interpolate the measured F_X to a fiducial epoch of 10 hr (hereafter, $F_{X,10}$), using the measured α_X when available, and the median of the distribution, $\langle\alpha_X\rangle = -1.33 \pm 0.38$ when a measurement is not available. The single exception is GRB 020405 for which the first measurement was obtained $t \approx 41$ hr, while the inferred jet break time is about 23 hr (Berger et al. 2003d). In this case, we extrapolate to $t = 10$ hr using $\alpha_X = -1.69$ for $t > 23$ hr and $\alpha_X = -0.78$ for $t < 23$ hr. We list the values of $F_{X,10}$ in Table 4.2.

In Figure 4.1 we plot the resulting distribution of $F_{X,10}$. For comparison we also show the distribution of γ-ray fluences from the sample presented by Bloom et al. (2001) and updated from the literature. Clearly, while the distribution of X-ray fluxes is narrower than that of the γ-ray fluences, $\sigma_l(f_\gamma) = 0.79^{+0.10}_{-0.08}$, it still spans ~ 2.5 orders of magnitude, i.e., $\sigma_l(F_{X,10}) = 0.57^{+0.07}_{-0.06}$. The value of $\sigma_l(F_{X,10})$, and all variances quoted below, are calculated by summing the Gaussian distribution for each measurement, and then fitting the combined distribution with a Gaussian profile.

We translate the observed X-ray fluxes to isotropic luminosities using:

$$L_{X,\rm iso}(t = 10\,{\rm hr}) = 4\pi d_L^2 F_{X,10}(1+z)^{\alpha_X - \beta_X - 1}. \quad (4.1)$$

We use $\beta_X \approx -1.05$, the weighted mean value for X-ray afterglows (De Pasquale et al. 2002), and the median redshift, $\langle z\rangle = 1.1$, for bursts that do not have a measured redshift. The resulting distribution of $L_{X,\rm iso}$, $\sigma_l(L_{X,\rm iso}) = 0.68^{+0.17}_{-0.09}$, is wider than that of F_X due to the dispersion in redshifts. We note that this is wider than the value quoted by Piran et al. (2001) of $\sigma_l(L_{X,\rm iso}) \approx 0.43$ based on a smaller sample, and ignoring the dispersion in redshift. Using the same method we find $\sigma_l(E_{\gamma,\rm iso}) = 0.92^{+0.12}_{-0.08}$.

In the absence of a strong correlation between f_b and $L_{X,\rm iso}$, the above results indicate that the distribution of the true X-ray luminosities, $L_X \equiv f_b^{-1} L_{X,\rm iso}$, should have a wider dispersion than either $L_{X,\rm iso}$ or f_b, for which we find $\sigma_l(f_b) = 0.52^{+0.13}_{-0.12}$ (Frail et al. 2001). Instead, when we apply the individual beaming corrections for those bursts that have a measured θ_j and redshift[1] (see Table 4.2), we find a significantly narrower distribution, $\sigma_l(L_X) = 0.32^{+0.10}_{-0.06}$.

SECTION 4.3

Beaming Corrections and Kinetic Energies

The reduced variance of L_X compared to that of $L_{X,\rm iso}$ requires a strong correlation between $L_{X,\rm iso}$ and f_b^{-1}, such that bursts with a brighter isotropic X-ray luminosity are also more strongly collimated. Indeed, as can be seen from Figure 4.2 the data exhibit such a correlation. Ignoring the two bursts which are obvious outliers (980326 and 990705), as well as GRBs 980329 and 980519, which do not

[1] These do not include GRB 990705 which is poorly characterized; see §4.3.

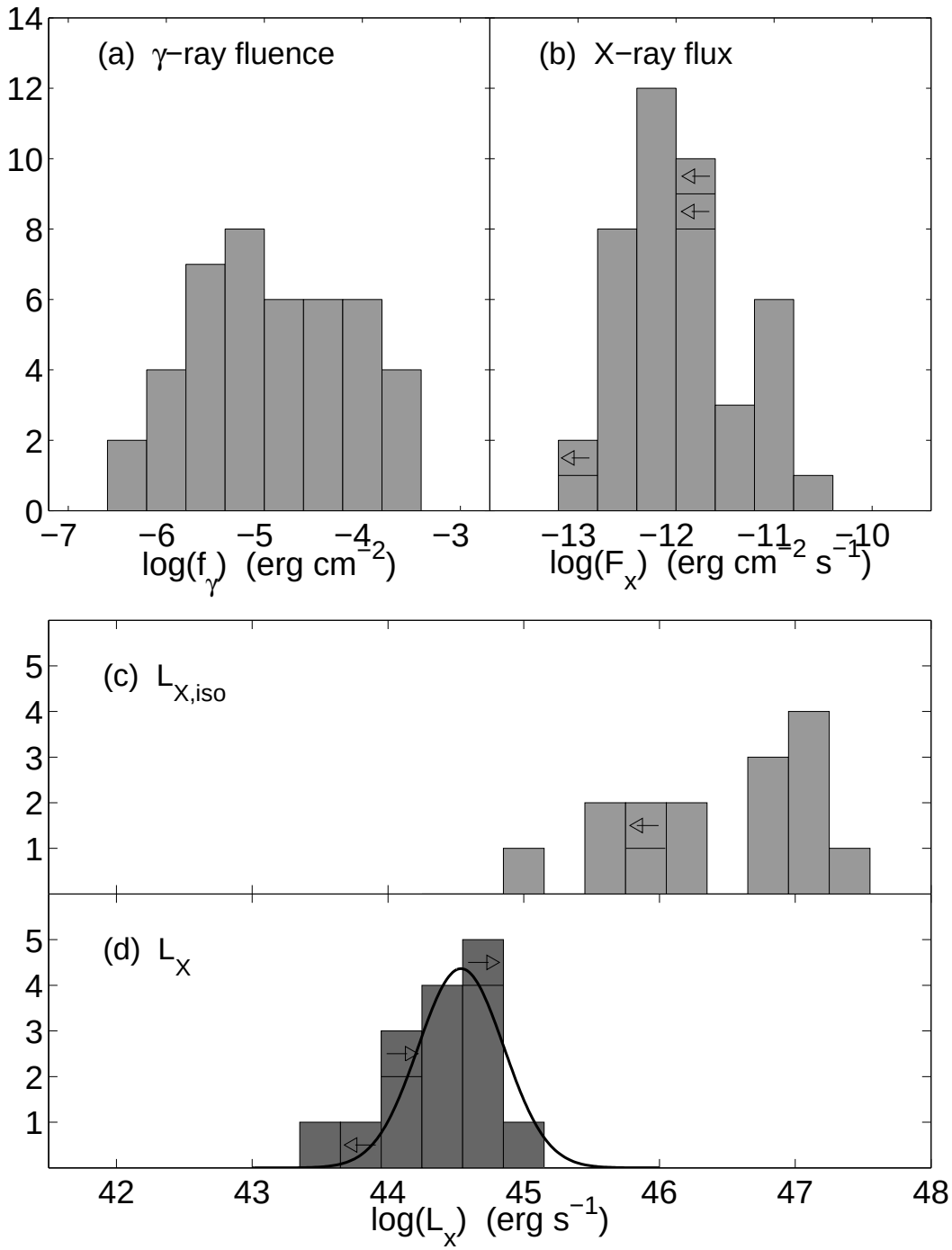

Figure 4.1: Panel (a) shows the distribution of γ-ray fluences. Panel (b) shows the distribution of X-ray fluxes scaled to $t = 10$ hr after the burst. In panel (c) we plot the isotropic-equivalent X-ray luminosity, $L_{X,\rm iso}$, for the subset of X-ray afterglows with known θ_j and redshift, while in panel (d) we show the true X-ray luminosity, $L_X = f_b^{-1} L_{X,\rm iso}$.

have a measured redshift, we find $L_{X,\rm iso} \propto f_b^{-0.80}$. The linear correlation coefficient between $\log(L_{X,\rm iso})$ and $\log(f_b^{-1})$ indicates a probability that the two quantities are not correlated of only 4.6×10^{-4}. For $\log(E_{\gamma,\rm iso})$ and $\log(f_b^{-1})$ we find a similar probability of 4.2×10^{-4} that the two quantities are not correlated.

Thus, as with the γ-ray emission, the observed afterglow emission also exhibits strong luminosity

diversity due to strong variations in f_b. Therefore, the mystery of GRBs is no longer the energy release but understanding what aspect of the central engine drives the wide diversity of f_b.

We note that there are four possible outliers in the correlation between $L_{X,\rm iso}$ and f_b^{-1}. The afterglows of GRBs 980326 and 980519 exhibit rapid fading (Groot et al. 1998; Vrba et al. 2000), which has been interpreted as the signature of an early jet break. However, it is possible that the rapid fading is instead due to a $\rho \propto r^{-2}$ density profile, and in fact for GRB 980519 such a model indicates $\theta_j \approx 0.12$, three times wider than in the constant density model. This is sufficient to bring GRB 980519 into agreement with the observed correlation. The redshift of GRB 980329 is not known, but with $z = 2$ it easily agrees with the correlation. Finally, the X-ray flux and jet opening angle for GRB 990705 are poorly characterized due to contamination from a nearby source (De Pasquale et al. 2002) and a poor optical light curve (Masetti et al. 2000b).

SECTION 4.4

Discussion and Conclusions

We have presented a comprehensive compilation of early X-ray observations of 41 GRBs, from which we infer $F_{X,10}$, the flux in the 2–10 keV band at 10 hr. As first pointed by Kumar (2000) and Freedman & Waxman (2001), the afterglow luminosity above the cooling frequency is $L_{X,iso} \propto \epsilon_e E_{b,\rm iso}$ where $E_{b,\rm iso}$ is the isotropic-equivalent explosion kinetic energy. More importantly, the flux is independent of the ambient density and weakly dependent on ϵ_B. For all well-modeled afterglows, the cooling frequency at 10 hr is below the X-ray band. Thus, $F_{X,10}$ can be utilized to yield information about the kinetic energy of GRBs.

Earlier work (Piran et al. 2001) focussed on statistical studies of $F_{X,10}$ and found the very surprising result that it is narrowly clustered. By assuming that the true kinetic energy, $E_b = E_{b,\rm iso} f_b \propto L_X = L_{X,\rm iso} f_b$, and f_b (the beaming factor) are uncorrelated, the authors deduced that L_X and thus E_b are even more strongly clustered. However, this approach is weakened by assuming (in effect) the answer. Furthermore, the approach of Piran et al. (2001) which relies on subtracting variances is very sensitive to measurement errors. To illustrate this point, we note $\sigma_l^2(L_{X,\rm iso}) = 0.68^{+0.17}_{-0.09}$ for the entire sample presented here, whereas $\sigma_l^2(f_b) = 0.52^{+0.13}_{-0.12}$. Thus, $\sigma_l^2(L_X) = 0.16^{+0.30}_{-0.21}$ may be negative using the statistical approach.

In contrast to the statistical approach, we take the direct approach and estimate the true kinetic energy, $E_b \propto L_{X,\rm iso} f_b$, by using the measured $L_{X,\rm iso}$ and inferred f_b. The advantage of our approach is that we do not make assumptions of correlations (or lack thereof) and more importantly we do not subtract variances. We directly compute the variance of the desired physical quantity, namely L_X, and find that it is strongly clustered.

Even more importantly, with our direct approach we have uncovered the physical reason for the wide dispersion in $L_{X,\rm iso}$ and the clustering of L_X, namely the dispersion in jet opening angles.

L_X is related to the physical quantities as follows (Freedman & Waxman 2001):

$$\epsilon_e E_b \propto A L_X Y^\epsilon, \tag{4.2}$$

where

$$Y \equiv B \epsilon_e^{-3} \epsilon_B^{-1} L_{X,\rm iso}^{-1}. \tag{4.3}$$

Here $\epsilon \equiv (p-2)/(p-1)$, as well as A and B depend to some extent on the details of the electron distribution (power law versus relativistic Maxwellian; the value of power law index, p).

There is no reason to expect that L_X should be clustered. However, one can argue that the microphysics should be the same for each GRB afterglow, in particular ϵ_e and p. The best studied afterglows appear to favor $p = 2.2$ (e.g., Frail et al. 2000c; Galama et al. 1998d), a value also favored by our current theoretical knowledge of shock acceleration (see Ostrowski & Bednarz 2002 and references therein). In addition, as already indicated by the γ-ray observations, there is evidence supporting strong clustering

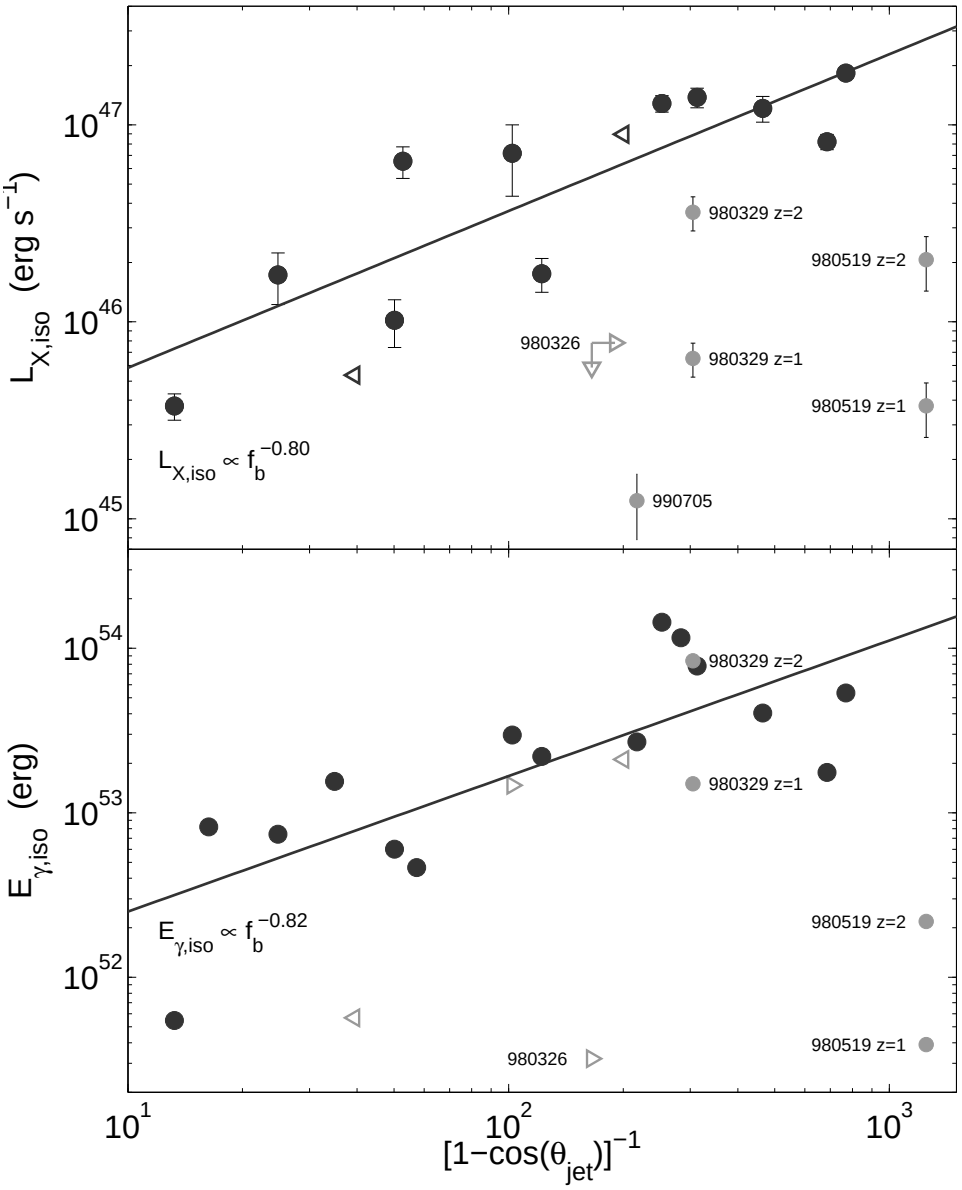

Figure 4.2: Isotropic-equivalent X-ray luminosity (top) and isotropic-equivalent γ-ray energy (bottom) as a function of the beaming factor, $[1 - \cos(\theta_j)]^{-1}$. There is a strong positive correlation between $L_{X,\rm iso}$ and f_b^{-1}, as well as between $E_{\gamma,\rm iso}$ and f_b^{-1} resulting in an approximately constant true X-ray luminosity and γ-ray energy release. In fact, while the distributions of all three parameters span about three orders of magnitude, the distributions of the beaming-corrected parameters span about one order of magnitude.

of explosion energies in GRBs (Frail et al. 2001).

Given these reasonable assumptions, a strong clustering of L_X makes sense if the physical quantities that are responsible for L_X are clustered. As can be seen from Equation 4.2, this would require that L_X be linearly related to E_b. Such a relation is possible if four conditions are met.

First, the afterglow X-ray emission on timescales of 10 hr must be primarily dominated by synchrotron emission (which is the basis of Equation 4.2). Contribution from inverse Compton (IC) emission, which depends strongly on n_0 and ϵ_B (Sari & Esin 2001), is apparently not significant. A possible exception is GRB 000926 (Harrison et al. 2001), but even there the IC contribution is similar to that from synchrotron emission.

Second, the energy radiated by the afterglow from the time of the explosion to $t = 10$ hr cannot be significant. This constrains the radiative losses at early time to at most a factor of few.

Third, p must be relatively constant (as one may expect in any case from insisting that the microphysics should not be different for different bursts). For example, changing p from a value of 1.5 to 3 results in Y^ϵ ranging from 0.003 to 117, a factor of 39,000! Even small changes in p, e.g., from $p = 1.75$ to $p = 2.25$, result in a factor of 8 change in Y^ϵ. In contrast, some afterglow models yield values of p significantly below 2 (e.g., Panaitescu & Kumar 2002), while others have p approaching 3 (Chevalier & Li 2000). Our results, on the other hand, indicate that one should set $p \approx 2$ and attribute apparent deviant values of p to external environment or energy injection from the central source.

Finally, since both the prompt and afterglow emission exhibit a strong correlation with f_b, which is determined from late-time observations (hours to weeks after the burst), the resulting constancy of both E_γ and E_b, indicates that GRB jets must be relatively homogeneous and maintain a simple conical geometry all the way from internal shocks ($\sim 10^{13} - 10^{14}$ cm) to the epoch of jet break ($\sim 10^{17}$ cm). This rules out the idea that brighter bursts are due to bright spots along specific lines of sight (Kumar & Piran 2000). At the same time, the possible deviation from a linear relation between $\log(L_{X,\rm iso})$ and $\log(f_b^{-1})$ may hold a clue to the structure of the jet.

With the result that GRB afterglows have a standard kinetic energy firmly established, the next step is to closely investigate bursts that deviate from this relation; such sources may be a clue to sub-classes of GRBs (e.g., Bloom et al. 2003b). Fortunately, while the statistical study of afterglow energetics used previously misses this point completely, the direct method employed in this paper can easily uncover these sources. More importantly, this method provides a framework for undrestanding the underlying physical processes which may give rise to such a diversity.

SRK thanks S. Phinney for valuable discussions. We also thank D. Lazzati, B. Zhang, and the anonymous referee for valuable comments. We acknowledge support from NSF and NASA grants.

Table 4.1. X-ray Afterglow Data

GRB	z	Epoch (hrs)	Flux (10^{-13} erg/cm^2/s)	α_X	$\theta_{\rm jet}$	Ref.	GRB	z	Epoch (hrs)	Flux (10^{-13} erg/cm^2/s)	α_X	$\theta_{\rm jet}$	Ref.
970111	···	24.0	1.05 ± 0.46	-0.4 ± 3.2^a	···	1,2	990510		17.1	18.5 ± 3.1			17
		30.7	0.95 ± 0.34		···	2			19.1	20.9 ± 2.3			17
970228	0.695	8.5	33.8 ± 3.3	-1.27 ± 0.14	···	2,3			24.0	12.1 ± 1.4			17
		12.7	28 ± 4			2			26.3	9.9 ± 1.1			17
		92.4	1.5 ± 0.4			2			29.4	7.8 ± 1.1			17
970402	···	9.9	2.9 ± 0.4	-1.35 ± 0.55	···	2	990627	···	11.9	3.5	···	···	18
		16.8	1.5 ± 0.4			2	990704	···	10.1	10.1 ± 2.9	-1.3 ± 0.3	···	19
970508	0.835	13.1	7.13	-1.1 ± 0.1	0.391	4,5			13.4	8.9 ± 2.2			19
		72.3	4.3 ± 0.5			2			23.3	3.1 ± 2.0			19
		104	2.3 ± 0.7			2			26.8	2.9 ± 1.6			19
970815	···	89.6	< 1	···	···	6	990705	0.840	14.5	1.9 ± 0.6	···	0.096	5,20
970828	0.958	4.0	118	-1.42	0.128	5,7	990806	···	13.6	5.5 ± 1.5	-1.4 ± 0.7	···	21
		42.6	4.1			7			34.3	1.5 ± 0.6			21
971214	3.418	8.1	9.0 ± 0.9	-1 ± 0.2	> 0.100	2,5	990907	···	11	10.2 ± 5.6	···	···	12
		28.9	2.1 ± 0.4			2	991014	···	11	$4.0^{+1.4}_{-1.2}$	···	···	12
971227	···	16.5	2.5 ± 0.7	-1.12 ± 0.06	···	8	991216	1.020	4.0	1240 ± 40	-1.61 ± 0.07	0.051	5,14,22
980326	$\sim 1^b$	8.5	< 16	···	< 0.110	9			10.9	250 ± 10			22
980329	···	8.4	14 ± 2.1	-1.55 ± 0.3	0.081	10,11	000115	···	2.9	270	< -1	···	23
		11.8	6.2 ± 1.2			10	000210	0.846	11	4.0 ± 1.0	-1.38 ± 0.03	···	24
		16.4	3.4 ± 1.0			10	000214	···	14.9	5	-1.8	···	25
		23.7	2.7 ± 0.7			10			22.1	2.5			25
		43.6	1.1 ± 0.4			10	000528	···	11	2.3 ± 1.0	···	···	12
980515	···	11	$2.0^{+0.5}_{-0.9}$	···	···	12	000529	···	9.0	2.8	···	···	26
980519	$< 2^c$	10.9	5.3 ± 1.0	-1.7 ± 0.7	0.040	13,14	000926	2.037	54.9	2.23 ± 0.77	-3.7 ± 1.5^a	0.140	14,27
		15.3	2.0 ± 0.4			13			66.5	0.94 ± 0.14			27
		21.5	1.6 ± 0.5			13	001025	···	50.4	0.53 ± 0.10	-3 ± 1.9^a	···	28
		27.2	0.8 ± 0.4			13	001109	···	19.3	7.1 ± 0.5	···	···	29
980613	1.096	9.9	7.1 ± 1.9	-0.92 ± 0.62	> 0.226	2	010214	···	7.7	6	< -1.6	···	30
		23.4	4.0 ± 0.8			2			24.1	< 0.5			30
980703	0.966	34.0	4.0 ± 1	-1.24 ± 0.18	0.200	2,15	010220	···	20.8	0.33	-1.2 ± 1.0	···	28
981226	···	14.0	4.0	-1.3 ± 0.4	···	16	010222	1.477	8.9	101 ± 11	-1.33 ± 0.04	0.080	14,31
990123	1.600	6.4	124 ± 11	-1.41 ± 0.05	0.089	2,5			32.7	18.7 ± 1.8			31
		23.4	19.1 ± 2.2			2			54.4	9.9 ± 0.5			31
990217	···	11	< 1.1	···	···	12	011211	2.14	11.0	1.9	-1.7 ± 0.2	···	32
990510	1.619	8.7	47.8 ± 3.1	-1.41 ± 0.18	0.054	5,14,17	020322	···	18.8	3.5 ± 0.2	-1.26 ± 0.23	···	33
		10.1	40.5 ± 2.6			17	020405	0.698	41.0	13.6 ± 2.5	-1.15 ± 0.95^d	0.285	34,35,36

Table 4.1

GRB	z	Epoch (hrs)	Flux (10^{-13} erg/cm^2/s)	α_X	$\theta_{\rm jet}$	Ref.	GRB	z	Epoch (hrs)	Flux (10^{-13} erg/cm^2/s)	α_X	$\theta_{\rm jet}$	Ref.
		11.7	32.8 ± 3.7			17	020813	1.254	31.9	22	-1.42 ± 0.05	0.066	37,38
		13.4	22.8 ± 2.8			17	021004	2.323	31.4	4.3 ± 0.7	-1.0 ± 0.2	0.240	39,40
		15.3	24.1 ± 2.7			17							

Note. — The columns are (left to right): (1) GRB name, (2) redshift, (3) mid-point epoch of X-ray observation, (4) X-ray flux, (5) temporal decay index ($F_X \propto t^{\alpha_X}$), (6) jet opening angle, and (7) references for the X-ray flux and jet opening angle. [a] Due to the large uncertainty in the value of α_X we use the median value for the sample, $\langle \alpha_X \rangle = -1.33 \pm 0.38$. [b] The redshift is based on matching the optical light curve of SN 1998bw to the red excess reported by Bloom et al. (1999). [c] The redshift limit is based on a detection of the afterglow in the optical U-band (Jaunsen et al. 2001). [d] The inferred jet break is at $t = 0.95$, prior to the X-ray observation — we use the model fit to extrapolate the flux to $t = 10$ hr (Berger et al. in prep.)

References. — (1) Feroci et al. (1998); (2) Piro (2001); (3) Frontera et al. (1998); (4) Piro et al. (1998); (5) Frail et al. (2001); (6) Murakami et al. (1997); (7) Smith et al. (2002a); (8) Antonelli et al. (1999); (9) Marshall & Takeshima (1998); (10) in 't Zand et al. (1998); (11) Yost et al. (2002); (12) De Pasquale et al. (2002); (13) Nicastro et al. (1999a); (14) Panaitescu & Kumar (2002); (15) Vreeswijk et al. (1999); (16) Frontera et al. (2000); (17) Pian et al. (2001); (18) Nicastro et al. (1999b); (19) Feroci et al. (2001); (20) Amati et al. (2000b); (21) Frontera et al. (1999); (22) Takeshima et al. (1999); (23) Marshall et al. (2000); (24) Piro et al. (2002); (25) Antonelli et al. (2000); (26) Feroci et al. (2000); (27) Harrison et al. (2001); (28) Watson et al. (2002); (29) Amati et al. (2000a); (30) Frontera et al. (2001); (31) in't Zand et al. (2001); (32) Reeves et al. (2002); (33) Watson et al. (2002); (34) Price & et al. (2002); (35) Mirabal et al. (2002); (36) Berger et al. (in prep); (37) Price et al. (2002a); (38) Vanderspek et al. (2002); (39) Fox et al. (in prep); (40) Frail et al. (in prep).

Table 4.2. X-ray Afterglow Data at $t = 10$ hr

GRB	z	$F_{X,10}$ (10^{-13} erg/cm^2/s)	$L_{X,iso}$ (10^{45} erg s^{-1})	$\theta_{\rm jet}$	L_X (10^{44} erg s^{-1})	GRB	z	$F_{X,10}$ (10^{-13} erg/cm^2/s)	$L_{X,iso}$ (10^{45} erg s^{-1})	$\theta_{\rm jet}$	L_X (10^{44} erg s^{-1})
970111	···	3.36 ± 1.64	2.56 ± 1.25	···	···	990806	···	8.46 ± 3.14	6.45 ± 2.39	···	···
970228	0.695	27.50 ± 3.17	6.82 ± 0.79	···	···	990907	···	11.58 ± 6.95	8.82 ± 5.29	···	···
970402	···	2.86 ± 0.61	2.18 ± 0.46	···	···	991014	···	4.54 ± 1.71	3.46 ± 1.30	···	···
970508	0.835	9.60 ± 1.47	3.74 ± 0.57	0.391	2.82 ± 0.43	991216	1.020	287.21 ± 14.73	183.22 ± 9.39	0.051	2.38 ± 0.12
970815	···	< 18.47	< 14.1	···	···	000115	···	78.3 ± 14.12	59.67 ± 10.76	···	···
970828	0.958	32.12 ± 6.31	17.6 ± 3.4	0.128	1.44 ± 0.28	000210	0.846	4.56 ± 1.16	1.83 ± 0.47	···	···
971214	3.418	7.29 ± 0.87	89.6 ± 10.8	> 0.100	> 4.48	000214	···	10.25 ± 2.16	7.81 ± 1.65	···	···
971227	···	4.38 ± 1.26	3.34 ± 0.96	···	···	000528	···	2.61 ± 1.27	1.99 ± 0.97	···	···
980326	~ 1	< 12.89	< 9.82	< 0.110	< 0.59	000529	···	2.43 ± 0.47	1.85 ± 0.36	···	···
980329	···	10.68 ± 2.10	8.14 ± 1.60	0.081	0.27 ± 0.05	000926	2.037	20.41 ± 8.06	71.69 ± 28.31	0.140	7.01 ± 2.77
980515	···	2.27 ± 0.90	1.73 ± 0.69	···	···	001025	···	67.85 ± 51.48	51.71 ± 39.22	···	···
980519	···	6.14 ± 1.89	4.68 ± 1.44	0.040	0.04 ± 0.01	001109	···	17.02 ± 2.06	12.97 ± 1.57	···	···
980613	1.096	7.03 ± 2.28	5.36 ± 1.74	> 0.226	> 1.36	010214	···	3.95 ± 0.80	3.01 ± 0.61	···	···
980703	0.966	18.24 ± 4.97	10.2 ± 2.8	0.200	2.03 ± 0.55	010220	···	0.79 ± 0.21	0.61 ± 0.16	···	···
981226	···	6.19 ± 1.20	4.72 ± 0.92	···	···	010222	1.477	86.50 ± 9.88	137.86 ± 15.75	0.080	4.41 ± 0.50
990123	1.600	66.09 ± 6.33	128.31 ± 12.29	0.089	5.08 ± 0.49	011211	2.14	2.23 ± 0.39	8.86 ± 1.56	···	···
990217	···	< 1.25	< 0.95	···	···	020322	···	7.75 ± 0.67	5.91 ± 0.51	···	···
990510	1.619	41.07 ± 3.68	82.09 ± 7.35	0.054	1.20 ± 0.11	020405	0.698	68.98 ± 20.21	17.29 ± 5.07	0.285	6.98 ± 2.04
990627	···	4.41 ± 0.85	3.36 ± 0.65	···	···	020813	1.254	113.98 ± 17.01	121.21 ± 18.09	0.066	2.61 ± 0.39
990704	···	10.23 ± 3.34	7.80 ± 2.54	···	···	021004	2.323	13.50 ± 2.47	65.36 ± 11.95	0.240	18.7 ± 3.4
990705	0.840	3.11 ± 1.14	1.23 ± 0.45	0.096	0.06 ± 0.02						

Note. — The columns are (left to right): (1) GRB name, (2) redshift, (3) X-ray flux at $t = 10$ hr, (4) X-ray luminosity at $t = 10$ hr, (5) jet opening angle, and (6) beaming-corrected X-ray luminosity at $t = 10$ hr.

CHAPTER 5

The Non-Relativistic Evolution of GRBs 980703 and 970508: Beaming-Independent Calorimetry

E. Berger[a], S. R. Kulkarni[a], & D. A. Frail[b]

[a]Department of Astronomy, 105-24 California Institute of Technology, Pasadena, CA 91125, USA

[b]National Radio Astronomy Observatory, P. O. Box 0, Socorro, NM 87801

Abstract

We use the Sedov-Taylor self-similar solution to model the radio emission from the γ-ray bursts (GRBs) 980703 and 970508, when the blastwave has decelerated to non-relativistic velocities. This approach allows us to infer the energy independent of jet collimation. We find that for GRB 980703 the kinetic energy at the time of the transition to non-relativistic evolution, $t_{\rm NR} \approx 40$ d, is $E_{\rm ST} \approx (1-6) \times 10^{51}$ erg. For GRB 970508 we find $E_{\rm ST} \approx 3 \times 10^{51}$ erg at $t_{\rm NR} \approx 100$ d, nearly an order of magnitude higher than the energy derived in Frail et al. (2000c). This is due primarily to revised cosmological parameters and partly to the maximum likelihood fit we use here. Taking into account radiative losses prior to $t_{\rm NR}$, the inferred energies agree well with those derived from the early, relativistic evolution of the afterglow. Thus, the analysis presented here provides a robust, geometry-independent confirmation that the energy scale of cosmological GRBs is about 5×10^{51} erg, and additionally shows that the central engine in these two bursts did not produce a significant amount of energy in mildly relativistic ejecta at late time. Furthermore, a comparison to the prompt energy release reveals a wide dispersion in the γ-ray efficiency, strengthening our growing understanding that E_γ is a not a reliable proxy for the total energy.

SECTION 5.1

Introduction

The two fundamental quantities in explosive phenomena are the kinetic energy, E_K, and the mass of the explosion ejecta, $M_{\rm ej}$, or equivalently the expansion velocity, $\beta \equiv v/c$, or Lorentz factor, $\Gamma = (1-\beta^2)^{-1/2}$. Together, these gross parameters determine the appearance and evolution of the resulting explosion. Gamma-ray bursts (GRBs) are distinguished by a highly relativistic initial velocity, $\Gamma_0 \gtrsim 100$, as inferred from their nonthermal prompt emission (Goodman 1986; Paczynski 1986). For the range of γ-ray isotropic-equivalent energies observed in GRBs, $E_{\gamma,{\rm iso}} \sim 10^{51} - 10^{54}$ erg (Bloom et al. 2001), this indicates $M_{\rm ej} \sim 10^{-5} - 10^{-3}$ M$_\odot$, compared to several M$_\odot$ in supernovae (SNe).

The true energy release of GRBs depends sensitively on the geometry of the explosion. For a collimated outflow ("jet") with a half-opening angle θ_j, it is $E = f_b E_{\rm iso}$, where $f_b \equiv [1 - \cos(\theta_j)]$ is the beaming fraction; the true ejecta mass is also a factor of f_b lower. Over the past several years there has been growing evidence for such collimated outflows coming mainly from achromatic breaks in the afterglow light curves (e.g., Kulkarni et al. 1999a; Stanek et al. 1999). The epoch at which the break occurs, t_j, corresponds to the time at which the ejecta bulk Lorentz factor decreases below θ_j^{-1} (Rhoads 1999; Sari et al. 1999).

In this context, several studies have shown that the beaming-corrected energies of most GRBs, in both the prompt γ-rays and afterglow phase, are of the order of 10^{51} erg (Frail et al. 2001; Panaitescu & Kumar 2002; Berger et al. 2003a; Bloom et al. 2003b; Yost et al. 2003). The various analyses are sensitive to the energy contained in ejecta with different velocities, $\Gamma \gtrsim 100$ in the γ-rays, $\Gamma \gtrsim 10$ in the early X-rays, and $\Gamma \gtrsim$ few in the broad-band afterglow. However, *none* are capable of tracing the existence and energy of non-relativistic ejecta.

Frail et al. (2000c) overcame this problem in the case of GRB 970508 by modeling the afterglow radio emission in the non-relativistic phase, thus inferring $E_K \approx 5 \times 10^{50}$ erg. This analysis has two significant advantages. First and foremost it is independent of jet collimation since the blastwave approaches spherical symmetry on the same timescale that it becomes non-relativistic (Livio & Waxman 2000). Second, this analysis relies on the simple and well-understood Sedov-Taylor dynamics of spherical blastwaves, as opposed to the hydrodynamics of spreading relativistic jets. In addition, the peak of the synchrotron spectrum on the relevant timescale lies in the radio band where the afterglow is observable for several hundred days.

Two recent developments make similar analyses crucial. We now recognize that some GRBs are dominated by mildly relativistic ejecta (Berger et al. 2003c). For example, for GRB 030329 the kinetic energy inferred from the afterglow emission, $E_K(\Gamma \sim {\rm few}) \approx 5 \times 10^{50}$ erg (Berger et al. 2003c), was an order of magnitude higher than the γ-ray energy release (Price et al. 2003). Similarly, for GRB 980425 $E_\gamma \approx 8 \times 10^{47}$ erg (Galama et al. 1998b; Pian et al. 2000) was about 1% of the relativistic kinetic energy of the associated SN 1998bw, $E_K \approx 10^{50}$ erg (Kulkarni et al. 1998; Li & Chevalier 1999). This begs the question, is there even more energy emerging from the engine, either at the time of the burst or later on, at non-relativistic velocities?

Second, there is a growing interest in "unification models" for GRBs, X-ray flashes (XRFs) and core-collapse SNe of type Ib/c, relying primarily on energetics arguments. For example, Lamb et al. (2004) argue that GRBs and XRFs share an energy scale of $\sim 10^{49}$ erg, and that all type Ib/c SNe give rise to GRBs or XRFs. Both conclusions result from significantly smaller values of θ_j compared to those inferred in the past, such that the energy scale, $\propto \theta_j^2$, is lower by a factor of ~ 100 and the true GRB rate, $\propto \theta_j^{-2}$, matches locally the type Ib/c SN rate. Given the important ramifications of the GRB energy scale for progenitor scenarios we would like to independently address the question: Is the energy scale of cosmic explosions 10^{49} erg, implicating all type Ib/c SNe in the production of GRBs, or does it cluster on $\sim 10^{51}$ erg?

The answer will also provide an independent confirmation of the jet paradigm by comparison to the isotropic-equivalent energies. This is crucial since other explanations for the light curve breaks have been suggested, including changes in the density of the circumburst medium, a transition to a non-relativistic evolution on the timescale of a few days (due to a high circumburst density), and changes in the energy spectrum of the radiating electrons (Dai & Lu 2001; Panaitescu 2001; Wei & Lu 2002).

Here we address the possibility of significant contribution from non-relativistic ejecta and robustly determine the energy scale of GRBs independent of geometrical assumptions, using Very Large Array[1] radio observations of the afterglows of GRBs 970508 and 980703 in the non-relativistic phase. We generally follow the treatment of Frail et al. (2000c), but unlike these authors we carry out a full least-squares fit to the data.

[1] The VLA is operated by the National Radio Astronomy Observatory, a facility of the National Science Foundation operated under cooperative agreement by Associated Universities, Inc.

SECTION 5.2

The Non-Relativistic Blastwave and Fireball Calorimetry

The dynamical evolution of an ultra-relativistic blastwave expanding in a uniform medium (hereafter, *ISM*) is described in terms of its Lorentz factor, $\Gamma = (17E_{\rm iso}/8\pi nm_pc^2r^3)^{1/2}$, where r is the radius of the blastwave and n is the number density of the circumburst medium (Blandford & McKee 1976). This, along with the relation for the observer time, which for the line of sight to the center of the blastwave is $t \approx r/8\Gamma^2c$ (e.g., Sari 1997), determines the evolution of the radius and Lorentz factor. For a spherical blastwave the expansion will eventually become non-relativistic on a timescale[2] , $t_{\rm NR} \approx 65(E_{\rm iso,52}/n_0)^{1/3}$ d, determined by the condition that the mass swept up by the blastwave, $M_{\rm sw} \approx E_{\rm iso}/c^2$, where $M_{\rm sw}$.

An initially collimated outflow becomes non-relativistic at $t_{\rm NR} \approx 40(E_{\rm iso,52}/n_0)^{1/4}t_{j,d}^{1/4}$ d (Livio & Waxman 2000). Moreover, as the jet expands sideways (at $t \gtrsim t_j$) the outflow approaches spherical symmetry on a timescale, $t_s \approx 150(E_{\rm iso,52}/n_0)^{1/4}t_{j,d}^{1/4}$ d, similar to $t_{\rm NR}$. Thus, regardless of the initial geometry of the outflow the non-relativistic expansion is well-approximated as a spherical outflow. We note that this discussion can be generalized to a range of radial density profiles. Here, in addition to the *ISM* model, we focus on a density profile, $\rho = Ar^{-2}$ (hereafter, *Wind*), appropriate for mass loss with a constant rate, $\dot{M}_w$, and speed, v_w (Chevalier & Li 2000).

Following the transition to non-relativistic expansion, the dynamical evolution of the blastwave is described by the Sedov-Taylor self-similar solution (Sedov 1946; von Neumann 1947; Taylor 1950). In this case the radius of the shock is given by $r \propto (E_{\rm ST}t^2/A)^{1/(5-s)}$, with $\rho = Ar^{-s}$. Thus, in the *ISM* case $r \propto (E_{\rm ST}t^2/nm_p)^{1/5}$, while in the *Wind* case $r \propto (E_{\rm ST}t^2/A)^{1/3}$. The constant of proportionality, $\xi(\hat{\gamma})$, depends on the adiabatic index of the gas, $\hat{\gamma}$, and is equal to 1.05 in the *ISM* case and 0.65 in the *Wind* case for $\hat{\gamma} = 13/9$. The latter is appropriate for pressure equilibrium between relativistic electrons and non-relativistic protons[3] (Frail et al. 2000c). The circumburst material shocked by the blastwave is confined downstream to a thin shell of width r/η, with $\eta \approx 10$.

To calculate the synchrotron emission emerging from this shock-heated material we make the usual assumptions. First, the relativistic electrons are assumed to obey a power-law distribution, $N(\gamma) \propto \gamma^{-p}$ for $\gamma \geq \gamma_m$. Second, the energy densities in the magnetic field and electrons are assumed to be a non-varying fraction (ϵ_B and ϵ_e, respectively) of the shock energy density. Coupled with the synchrotron emissivity and taking into account self-absorption, the flux received by an observer at frequency ν and time t is given by (e.g., Frail et al. 2000c):

$$F_\nu = F_0(t/t_0)^{\alpha_F}[(1+z)\nu]^{5/2}(1-e^{-\tau})f_3(\nu/\nu_m)f_2^{-1}(\nu/\nu_m), \tag{5.1}$$

the optical depth is given by

$$\tau_\nu = \tau_0(t/t_0)^{\alpha_\tau}[(1+z)\nu]^{-(p+4)/2}f_2(\nu/\nu_m), \tag{5.2}$$

and the function

$$f_l(x) = \int_0^x F(y)y^{(p-l)/2}dy. \tag{5.3}$$

Here, $\nu_m = \nu_0(t/t_0)^{\alpha_m}/(1+z)$ is the synchrotron peak frequency corresponding to electrons with $\gamma = \gamma_m$, $F(y)$ is given in, e.g., Rybicki & Lightman (1979), and the temporal indices α_F, α_τ and α_m are determined by the density profile of the circumburst medium. In the *ISM* case $\alpha_F = 11/10$, $\alpha_\tau = 1 - 3p/2$, and $\alpha_m = -3$, while in the *Wind* case $\alpha_F = 11/6$, $\alpha_\tau = -1 - 7p/6$, and $\alpha_m = -7/3$ (Waxman 2004). Equations 5.1–5.3 include the appropriate redshift transformations to the rest-frame of the burst.

[2] Here and throughout the paper we use the notation $q = 10^x q_x$.

[3] The relative pressure between the protons and relativistic electrons depends on the fraction of energy in relativistic electrons, ϵ_e. If this fraction is low, the pressure may be dominated by the non-relativistic protons in which case $\hat{\gamma} = 5/3$. As we show below, ϵ_e for both GRB 980703 and GRB 970508 is in the range ~ 0.1 to 0.5 and thus $\hat{\gamma} = 13/9$ is applicable.

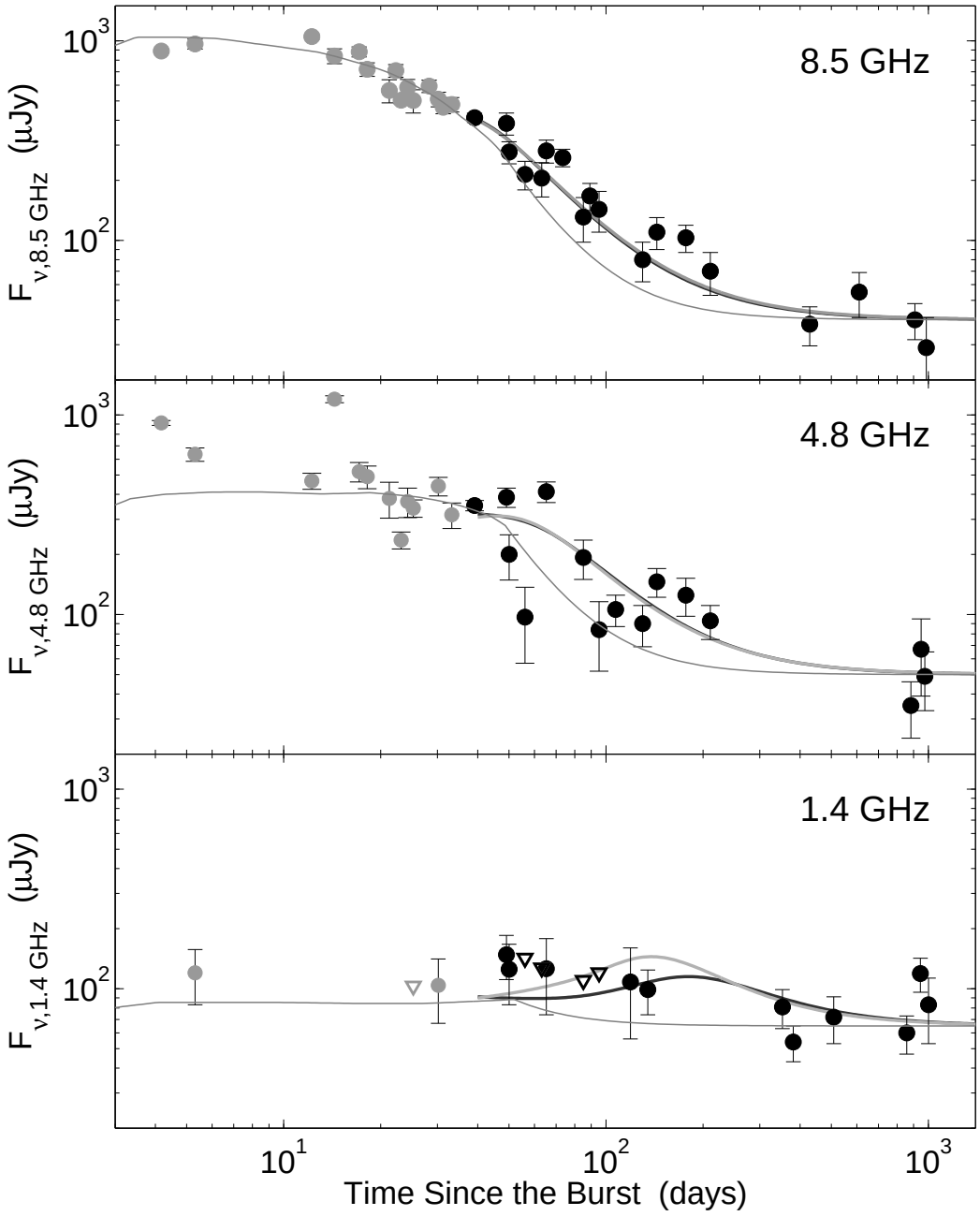

Figure 5.1: Radio light curves of the afterglow of GRB 980703 at 1.4, 4.9 and 8.5 GHz. Only data at $t \geq t_{\rm NR} = 40$ d (black circles) are used in the fit. The data exhibit a clear flattening relative to the relativistic evolution of the afterglow (thin gray line; Frail et al. 2003b) in agreement with the expected change from $F_\nu \propto t^{-p}$ (jet) to $F_\nu \propto t^{(21-15p)/10}$ (*ISM*) or $F_\nu \propto t^{(5-7p)/6}$ (*Wind*) in the non-relativistic regime. The best-fit light curves for the *ISM* (black) and *Wind* (gray) models are indistinguishable. The models include a contribution from the host galaxy of 40, 50 and 65 μJy at 8.5, 4.9 and 1.4 GHz, respectively.

Based on the temporal scalings the synchrotron flux in the optically-thin regime ($\nu \gg \nu_m, \nu_a$) evolves as $F_\nu \propto t^{(21-15p)/10}$ (*ISM*) or $F_\nu \propto t^{(5-7p)/6}$ (*Wind*); here the synchrotron self-absorption frequency, ν_a, is defined by the condition $\tau_\nu(\nu_a) = 1$. Thus, for $\nu \gg \nu_m, \nu_a$ the transition to non-relativistic expansion is manifested as a steepening of the light curves at $t_{\rm NR}$ if the outflow is spherical (Sari et al. 1998; Chevalier & Li 2000), or a flattening if the outflow was initially collimated (Sari et al. 1999). Below, we

use this behavior to estimate $t_{\rm NR}$ for GRBs 980703 and 970508/

In §5.3 and §5.4 we use the temporal decay indices and Equations 5.1–5.3 to carry out a least-squares fit to the data at $t > t_{\rm NR}$ with the free parameters F_0, τ_0, ν_0 and p. These parameters are in turn used to calculate the physical parameters of interest, namely r, n_e, γ_m and B; $n_e \approx (\eta/3)n$ is the shocked electron density (Frail et al. 2000c). Since only three spectral parameters are available, this leaves the radius unconstrained and thus,

$$B = 11.7(p+2)^{-2}F_{0,-52}^{-2}(r_{17}/d_{28})^4 \ {\rm G}, \tag{5.4}$$

$$\gamma_m = 6.7(p+2)F_{0,-52}\nu_{0,9}^{1/2}(r_{17}/d_{28})^{-2}, \tag{5.5}$$

$$n_e = 3.6\times10^{10}c_n\eta_1F_{0,-52}^3\nu_{0,9}^{(1-p)/2}\tau_{0,32}r_{17}^{-1}(r_{17}/d_{28})^{-6} \ {\rm cm}^{-3}, \tag{5.6}$$

$$c_n = (1.67\times10^3)^{-p}(5.4\times10^2)^{(1-p)/2}(p+2)^2/(p-1). \tag{5.7}$$

In the *Wind* model, the density is appropriate at $r_{\rm ST} \equiv r(t_{\rm NR})$, i.e., $\rho(r) = nm_p(r/r_{\rm NR})^{-2}$.

To determine the radius of the blastwave a further constraint is needed. We note that the energy contained in the electrons and magnetic field cannot exceed the thermal energy of the Sedov-Taylor blastwave, which accounts for about half of the total energy (Frail et al. 2000c). The energy in the electrons is given by $E_e = [(p-1)/(p-2)]n_e\gamma_m m_e c^2 V$, while the energy in the magnetic field is $E_B = B^2V/8\pi$; here $V = 4\pi r^3/\eta$ is the volume of the synchrotron emitting shell. Thus, using Equations 5.4–5.7 and the condition $E_e + E_B \leq E_{\rm ST}/2$ we can constrain the range of allowed values of r. In the *ISM* model $E_{\rm ST} = nm_p(r/1.05)^5[t_{\rm NR}/(1+z)]^{-2}$, while in the *Wind* model $E_{\rm ST} = A(r/0.65)^3[t_{\rm NR}/(1+z)]^{-2}$.

With a constraint on the radius we can also ensure self-consistency by calculating the velocity of the blastwave when it enters the Sedov-Taylor phase, $v_{\rm ST} = 2r(1+z)/5t_{\rm NR}$ (*ISM*) or $v_{\rm ST} = 2r(1+z)/3t_{\rm NR}$ (*Wind*). We expect that roughly $v \sim c$. Finally, the isotropic-equivalent mass of the ejecta is given by $M_{\rm ej} = 4\pi nm_p r_{\rm ST}^3$ (*ISM*) or $4\pi A r_{\rm ST}$ (*Wind*). The actual ejecta mass is reduced by a factor f_b relative to this value.

SECTION 5.3

GRB 980703

In Figure 5.1 we plot the radio light curves of GRB 980703. The data are taken from Berger et al. (2001b) and Frail et al. (2003b). Two gross changes in the light curves evolution are evident: a flattening at $t \approx 40$ d at 4.9 and 8.5 GHz and a transition to a constant flux density at late time. The latter is due to radio emission from the host galaxy of GRB 980703 with flux densities at 1.4, 4.9 and 8.5 GHz of 65, 50 and 40 μJy, respectively (Berger et al. 2001b). The flattening at $t \approx 40$ d marks the transition to non-relativistic evolution following a period of sideways expansion of the initially collimated outflow (Figure 5.1). A similar value, $t_{\rm NR} \approx 30 - 50$ d has been inferred by Frail et al. (2003b) from tracking the evolution of the blastwave Lorentz factor in the relativistic phase. We therefore use here $t_{\rm NR} = 40$ d.

We follow the method outlined in §5.2 using both the *ISM* and *Wind* cases. The results of both fits, shown in Figure 5.1, are overall indistinguishable. In what follows we quote the results of the *ISM* model. The best-fit parameters ($\chi^2_{\rm min} = 123$ for 45 degrees of freedom) are: $F_{0,-52} \approx 2.7$, $\tau_{0,32} \approx 80$, $\nu_{0,9} \approx 4.6$ and $p \approx 2.8$. The relatively large values of $\chi^2_{\rm min}$ is due primarily to fluctuations induced by interstellar scintillation, particularly at 4.9 GHz.

Using $d_{28} = d_{L,28}/(1+z)^{1/2} = 1.4$ ($z = 0.966$, $H_0 = 71$ km s^{-1} Mpc^{-1}, $\Omega_m = 0.27$ and $\Omega_\Lambda = 0.73$), and Equations 5.4–5.7 we find $B \approx 1.8\times10^{-2}r_{17}^4$ G, $\gamma_m \approx 300r_{17}^{-2}$, and $n_e \approx 4.9\times10^3 r_{17}^{-7}$ cm^{-3}. From these parameters we calculate $E_e \approx 3.4\times10^{51}r_{17}^{-6}$ erg, $E_B \approx 1.7\times10^{46}r_{17}^{11}$ erg, and $E_{\rm ST} \approx 6.2\times10^{51}r_{17}^{-2}$. These results are plotted in Figures 5.2 and 5.3.

The range of blastwave radii allowed by the constraint $E_e + E_B \lesssim E_{\rm ST}/2$ is $r_{17} \approx 1.05 - 2.5$, resulting in a range of values for the Sedov-Taylor energy, $E_{\rm ST} \approx (1-6)\times10^{51}$ erg. Given the strong

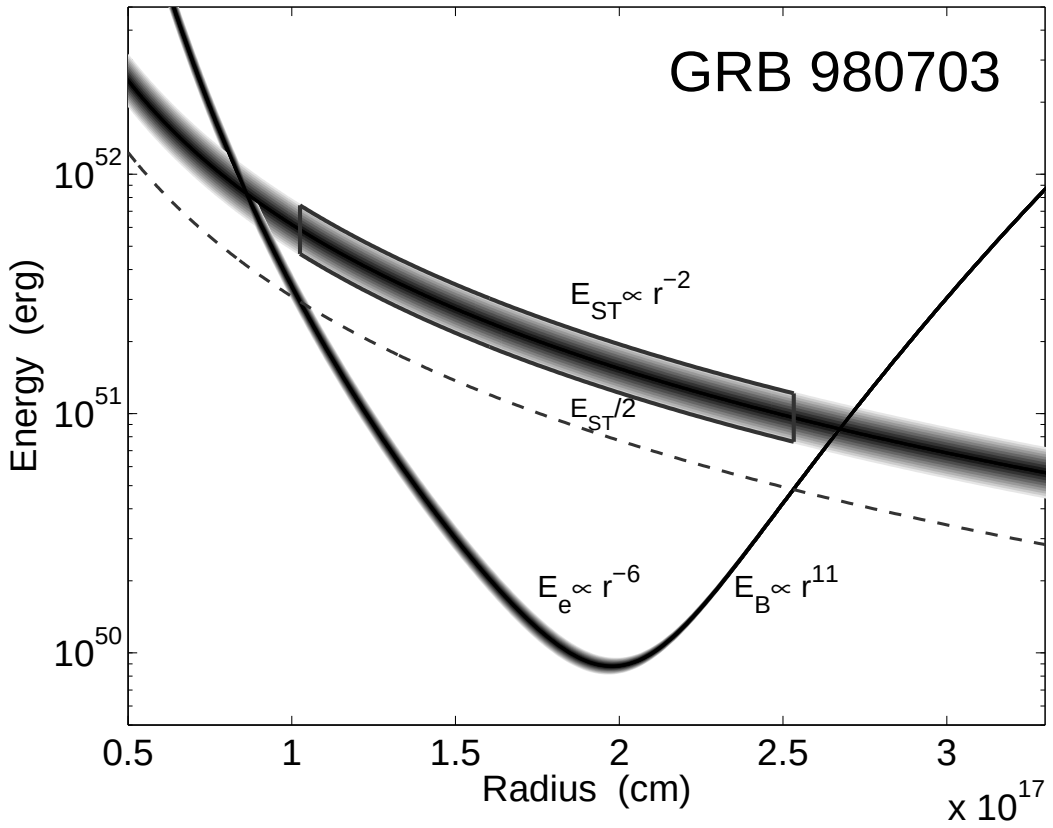

Figure 5.2: Energies associated with the afterglow of GRB 980703 in the non-relativistic Sedov-Taylor phase as a function of the (unconstrained) blastwave radius. The thin curve is the sum of the energy in relativistic electron ($E_e \propto r^{-6}$) and in the magnetic fields ($E_B \propto r^{11}$). Also plotted are the Sedov-Taylor energy ($E_{\rm ST} \propto r^{-2}$) and the thermal component, $E_{\rm ST}/2$. The shading corresponds to an uncertainty of 30% in the value of the synchrotron frequency ν_0 at $t = t_{\rm NR}$. The value of $E_{\rm ST}/2$ provides an additional constraint, $E_e + E_B \leq E_{\rm ST}/2$, which limits the range of allowed radii in the solution (boxed region).

dependence on radius, the ratio of energy in the electrons to the energy in the magnetic field ranges from $\epsilon_e/\epsilon_B \approx 0.03 - 9 \times 10^4$, while the specific values range from $\epsilon_e \approx 0.01 - 0.45$ and $\epsilon_B \approx 5 \times 10^{-6} - 0.4$. The circumburst density is in the range $n \approx 8 - 3.5 \times 10^3$ cm^{-3}, while the blastwave velocity is $\beta_{\rm ST} \approx 0.8 - 1.9$. Finally, the isotropic-equivalent mass of the ejecta ranges from $(1 - 40) \times 10^{-4}$ M$_\odot$.

A comparison to the values derived by Frail et al. (2003b) using modeling of the afterglow emission in the relativistic phase is useful. These authors find $n \approx 30$ cm^{-3}, $\epsilon_e \approx 0.27$ and $\epsilon_B \approx 2 \times 10^{-3}$. Using the same density in our model (Figure 5.3), as required by the *ISM* density profile, gives a radius $r_{17} \approx 1.75$ and hence $\epsilon_e \approx 0.06$ and $\epsilon_B \approx 4 \times 10^{-3}$, in rough agreement; the energy is $E_{\rm ST} \approx 2 \times 10^{51}$ erg.

If we assume alternatively that the energy in relativistic electrons and the magnetic field are in equipartition, we find $r_{17} \approx 2.05$. In this case, $E_{\rm ST} \approx 1.5 \times 10^{51}$ erg, $n \approx 10$ cm^{-3}, $B \approx 0.3$ G, and $\epsilon_e = \epsilon_B = 0.03$.

SECTION 5.4

GRB 970508

The non-relativistic evolution of GRB 970508 was studied by Frail et al. (2000c). These authors provide a rough model for the radio emission beyond $t_{\rm NR} \approx 100$ d and argue that the constraint $E_e + E_B \lesssim E_{\rm ST}/2$ requires the electron and magnetic field energy to be in equipartition, $\epsilon_e = \epsilon_B \approx 0.25$, with

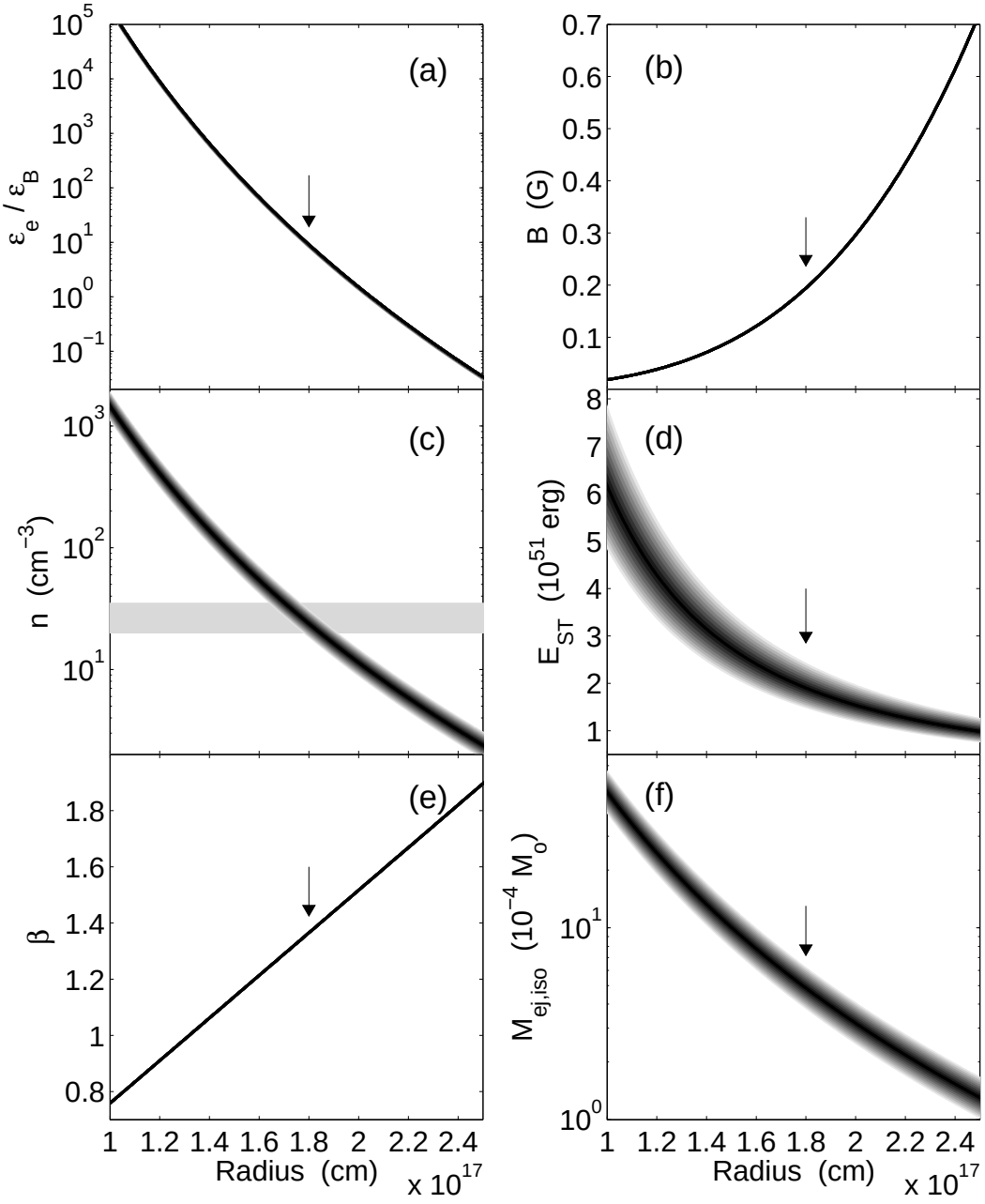

Figure 5.3: Physical parameters of the Sedov-Taylor blastwave for GRB 980703 at $t_{\rm NR} = 40$ d for the range of radii that obey the constraint $E_e + E_B \leq E_{\rm ST}/2$ (Figure 5.2): (a) The ratio of energy in the relativistic electrons to that in the magnetic fields, (b) the magnetic field strength, (c) the density of the circumburst medium, (d) the Sedov-Taylor energy, (e) the velocity of the blastwave, and (f) the isotropic-equivalent mass of the ejecta produced by the central engine and responsible for the afterglow emission. The light shaded region in (c) marks the range of densities inferred from the relativistic evolution of the fireball, $n \approx 20 - 35$ cm^{-3} (Frail et al. 2003b). With the additional constraint that the density derived here conform to this value, we derive the values of ϵ_e/ϵ_B, B, $E_{\rm ST}$, β, and $M_{\rm ej}$ marked by arrows.

$E_{\rm ST} \approx 4.4 \times 10^{50}$ erg. Here we perform a full least-squares fit, using $t_{\rm NR} = 100$ d, and find somewhat different results. We use $t_{\rm NR} \approx 100$ d, noting that for GRB 970508 the outflow appears to be weakly-collimated (Yost et al. 2003), and hence the transition is manifested as a mild steepening of the light

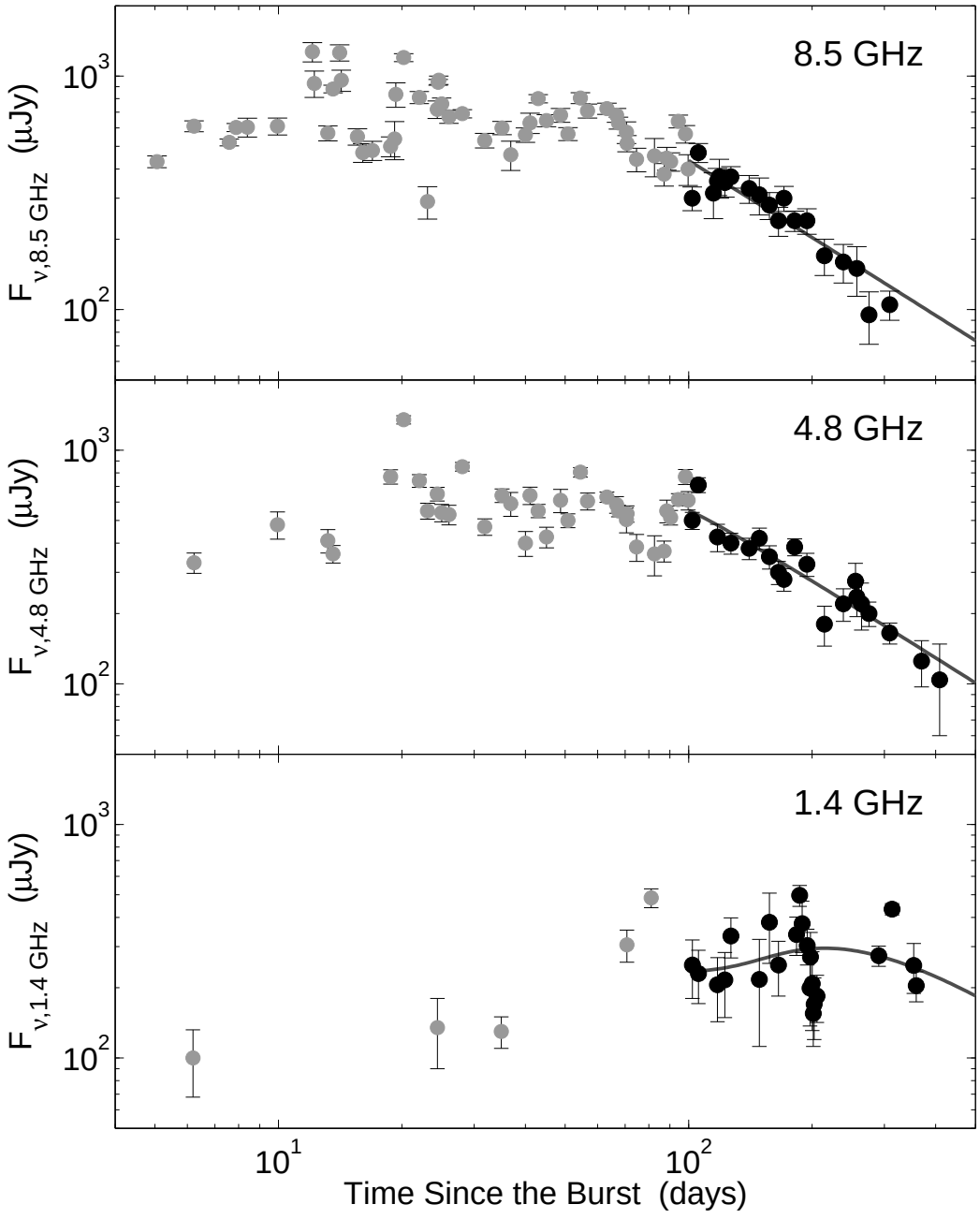

Figure 5.4: Radio light curves of the afterglow of GRB 970508 at 1.4, 4.9 and 8.5 GHz. Only data at $t \geq t_{\rm NR} = 100$ d (black circles) are used in the fit. The best-fit light curves for the *ISM* model are shown (black); the *Wind* model can be ruled out since it requires $p < 2$.

curves (see §5.2).

The best-fit parameters in the *ISM* model[4] ($\chi^2_{\rm min} = 164$ for 58 degrees of freedom) are: $F_{0,-52} \approx 38$, $\tau_{0,32} \approx 3.1 \times 10^{-3}$, $\nu_{0,9} \approx 3$ and $p \approx 2.17$. The large value of $\chi^2_{\rm min}$ is due primarily to interstellar scintillation.

In comparison, Frail et al. (2000c) use $F_{0,-52} \approx 41$, $\tau_{0,32} \approx 5.3 \times 10^{-3}$, $\nu_{0,9} \approx 9.5$, and they set $p = 2.2$; a solution with $\nu_{0,9} \approx 4.2$ is also advocated but it is not used to derive the physical parameters

[4] We do not consider the *Wind* case since in this model the observed decay rates at 4.9 and 8.5 GHz, $F_\nu \propto t^{-1.2}$, require $p \approx 1.7$ and hence an infinite energy. This can be avoided by assuming a break in the electron energy distribution at $\gamma_b > \gamma_m$ with a power law index $q > 2$, but we do not have the data required to constrain either γ_b or q.

of the blastwave. The formal χ^2 values for these solutions are 225 and 254, respectively, somewhat worse than the solution found here.

As a result, we find that solutions away from equipartition are allowed. Adopting the cosmological parameters used by Frail et al. (2000c), $H_0 = 70$ km s^{-1} Mpc^{-1}, $\Omega_m = 1$ and $\Omega_\Lambda = 0$, we find $E_{\rm ST} \approx (6-11)\times 10^{50}$ erg, a factor of about $20-100\%$ higher than the values inferred by these authors.

Using the currently favored cosmology (§5.3), we find instead that the distance to the burst is higher by about 30%, $d_{28} = 1.21$ compared to 0.94 (Frail et al. 2000c). The change in distance has a significant effect on the derived parameters since $E_e \propto d^8$, $E_B \propto d^{-8}$ and $E_{\rm ST} \propto n \propto d^6$. Thus, we find that the constraint on $E_e + E_B$ indicates $r_{17} \approx 3.7 - 5.9$ and therefore, $B \approx 0.04 - 0.25$ G, $\gamma \approx 65 - 165$ and $n \approx 0.4 - 10$ cm^{-3}. The Sedov-Taylor energy is $E_{\rm ST} \approx (1.5 - 3.8)\times 10^{51}$ erg, while $\epsilon_e \approx 0.07 - 0.5$ and $\epsilon_B \approx 0.001 - 0.45$ (Figures 5.5 and 5.6). Assuming equipartition, we find $r_{17} = 5.3$, $E_{\rm ST} = 1.8\times 10^{51}$ erg, and $\epsilon_e = \epsilon_b = 0.11$. The derived energy is about a factor of four higher than the previous estimate (Frail et al. 2000c).

A comparison of our best-fit model with the flux of the afterglow in the optical R-band at $t = 110$ d, $F_{\nu,R} \approx 0.3$ μJy (Garcia et al. 1998), indicates a break in the spectrum. If we interpret this break as due to the synchrotron cooling frequency, above which the spectrum is given by $F_\nu \propto \nu^{-p/2}$, we find $\nu_c \approx 6\times 10^{13}$ Hz. Since $\nu_c = 1.9\times 10^{10} B^{-3}(t/110\,{\rm d})^{-2}$ Hz we infer $B \approx 0.073$ G and hence $r_{17} = 4.3$, $E_{\rm ST} = 2.8\times 10^{51}$, $\epsilon_e = 0.25$ and $\epsilon_B = 8\times 10^{-3}$. These values are in rough agreement with those inferred from modeling of the relativistic phase (Panaitescu & Kumar 2002; Yost et al. 2003), although our value of ϵ_B is somewhat lower.

SECTION 5.5

Radiative Corrections

The energies derived in §5.3 and §5.4 are in fact lower limits on the initial kinetic energy of the blastwave due to synchrotron radiative losses. These play a role primarily in the fast-cooling regime ($\nu_c \ll \nu_m$), which dominates in the early stages of the afterglow evolution (e.g., Sari et al. 1998).

Yost et al. (2003) estimate the time at which fast-cooling ends, $t_{\rm cm} \approx 0.1$ and 1.4 days after the burst for GRB 970508 and GRB 980703, respectively. Using these values, and our best estimate of $\epsilon_e \approx 0.06$ (980703) and $\epsilon_e \approx 0.25$ (970508), we calculate the radiative corrections, $E \propto t^m$, going back from $t_{\rm NR}$ to about 90 s after the burst. Here $m \approx -17\epsilon/12$, with $\epsilon = \epsilon_e/(1 + 1.05\epsilon_e)$ for $t < t_{\rm cm}$ and it is quenched by a factor $(\nu_m/\nu_c)^{(p-2)/2} < 1$ at later times. Thus, at low values of ϵ_e the radiative losses are negligible. The cutoff at 90 s corresponds to the approximate deceleration time of the ejecta, $t_{\rm dec} \approx 90(E_{52}/n_0\Gamma_2^8)^{1/3}$ s.

We find that approximately 50% and 90% of the energy was radiated away before $t_{\rm NR}$ for GRBs 980703 and 970508, respectively. Thus, the initial kinetic energies are estimated to be 4×10^{51} erg and 3×10^{52} erg, respectively. The corrections from $t_{\rm NR}$ back to $t_{\rm cm}$, 10% for GRB 980703 and 70% for GRB 970508, indicate $E_K \approx 2\times 10^{51}$ and 9×10^{51} erg, respectively. Both estimates of the energy are in excellent agreement with those inferred from the relativistic evolution of the fireball at $t_{\rm cm}$ (Yost et al. 2003), $E_K \approx 3\times 10^{51}$ erg (980703) and $E_K \approx 1.2\times 10^{52}$ erg (970508).

SECTION 5.6

Discussion and Conclusions

Analysis of the synchrotron emission from a GRB blastwave in the non-relativistic phase has the advantage that it is independent of geometry and is described by the well-understood Sedov-Taylor self-similar solution. Using this approach to model the late-time radio emission from GRBs 980703 ($t > 40$ d) and 970508 ($t > 100$ d) we infer kinetic energies in the range $(1-6)\times 10^{51}$ erg and $(1.5-4)\times 10^{51}$ erg, respectively. Including the effect of radiative losses starting at $t_{\rm dec} \sim 90$ s, we find that the initial kinetic energies were about 4×10^{51} erg and 3×10^{52} erg, respectively.

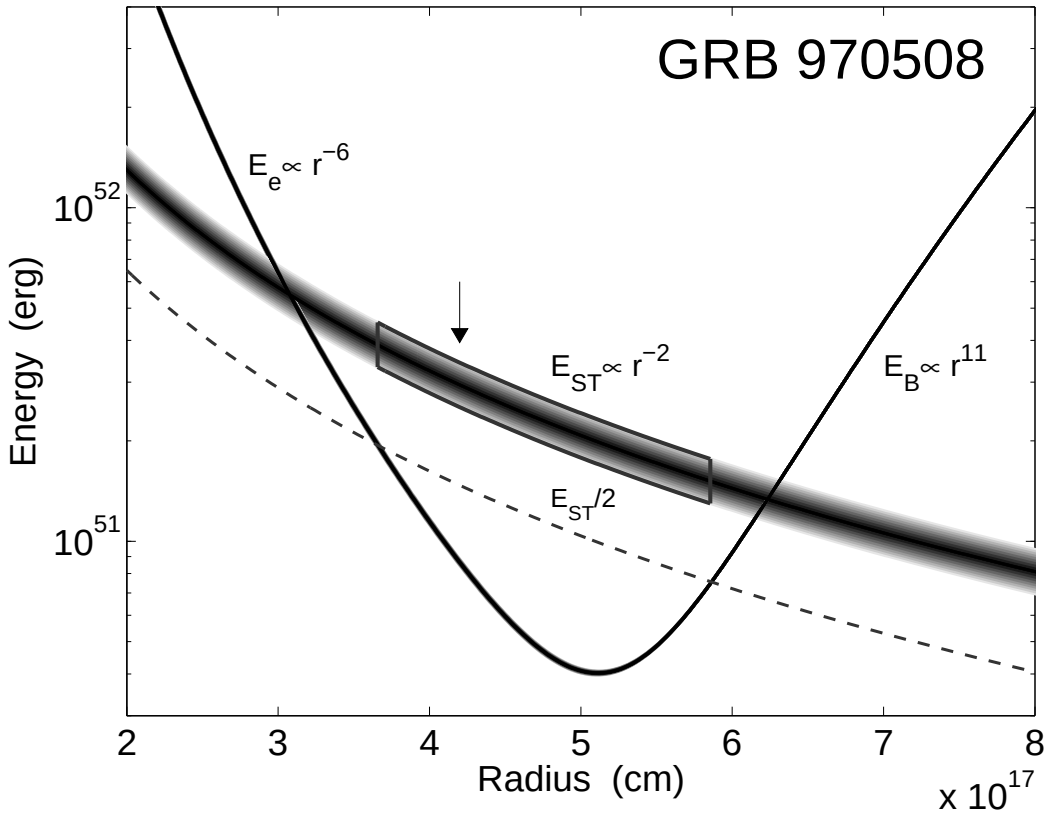

Figure 5.5: Energies associated with the afterglow of GRB 970508 in the non-relativistic Sedov-Taylor phase as a function of the (unconstrained) blastwave radius. The thin curve is the sum of the energy in relativistic electron ($E_e \propto r^{-6}$) and in the magnetic fields ($E_B \propto r^{11}$). Also plotted are the Sedov-Taylor energy ($E_{\rm ST} \propto r^{-2}$) and the thermal component, $E_{\rm ST}/2$. The shading corresponds to an uncertainty of 30% in the value of the synchrotron frequency ν_0 at $t = t_{\rm NR}$. The value of $E_{\rm ST}/2$ provides an additional constraint, $E_e + E_B \leq E_{\rm ST}/2$, which limits the range of allowed radii in the solution (boxed region). Finally, the arrow marks the most likely solution using the value of the cooling frequency as estimated from a combination of the radio and optical data (§5.4). This additional parameter breaks the radius degeneracy, indicating $r \approx 4.2 \times 10^{17}$ cm and $E_{\rm ST} \approx 3 \times 10^{51}$ erg

The inferred kinetic energies confirm, independent of any assumptions about the existence or opening angles of jets, that the energy scale of GRBs is $\sim 5 \times 10^{51}$ erg. We therefore unambiguously rule out the recent claim of Lamb et al. (2004) that the energy scale of GRBs is of the order of 10^{49} erg. Since the claimed low energies were based on the apparent correlation between $E_{\gamma,{\rm iso}}$ and the energy at which the prompt emission spectrum peaks, $E_{\rm peak}$ (Amati et al. 2002), we conclude that this relation, and the prompt emission in general, does not provide a reliable measure of the total energy. As a corollary, we rule out the narrow jet opening angles used by Lamb et al. (2004), $\theta_j \sim 0.1^{\rm o}$ and thus confirm that the true GRB rate is significantly lower than the rate of type Ib/c SNe (Berger et al. 2003b).

Finally, the overall agreement between the energies derived here and those inferred from modeling of the relativistic phase of the afterglow indicates that the central engine in GRBs 980703 and 970508 did not produce a significant amount of energy in mildly relativistic ejecta ($\Gamma\beta \gtrsim 2$) at late time, $t \sim t_{\rm NR}$. However, a comparison to the beaming-corrected γ-ray energies (Bloom et al. 2003b), $E_\gamma \approx 1.1 \times 10^{51}$ erg (GRB 980703) and $E_\gamma \sim 10^{51}$ erg (GRB 970508) reveals that the efficiency of the blastwave in producing γ-rays, ϵ_γ, varies considerably: $\sim 20\%$ for GRB 980703, but only $\sim 3\%$ for GRB 970508. The wide dispersion in ϵ_γ strengthens the conclusion that E_γ is not a reliable tracer of the total energy (Berger et al. 2003c).

The low value of ϵ_γ for GRB 970508 may indicate an injection of energy from mildly relativistic

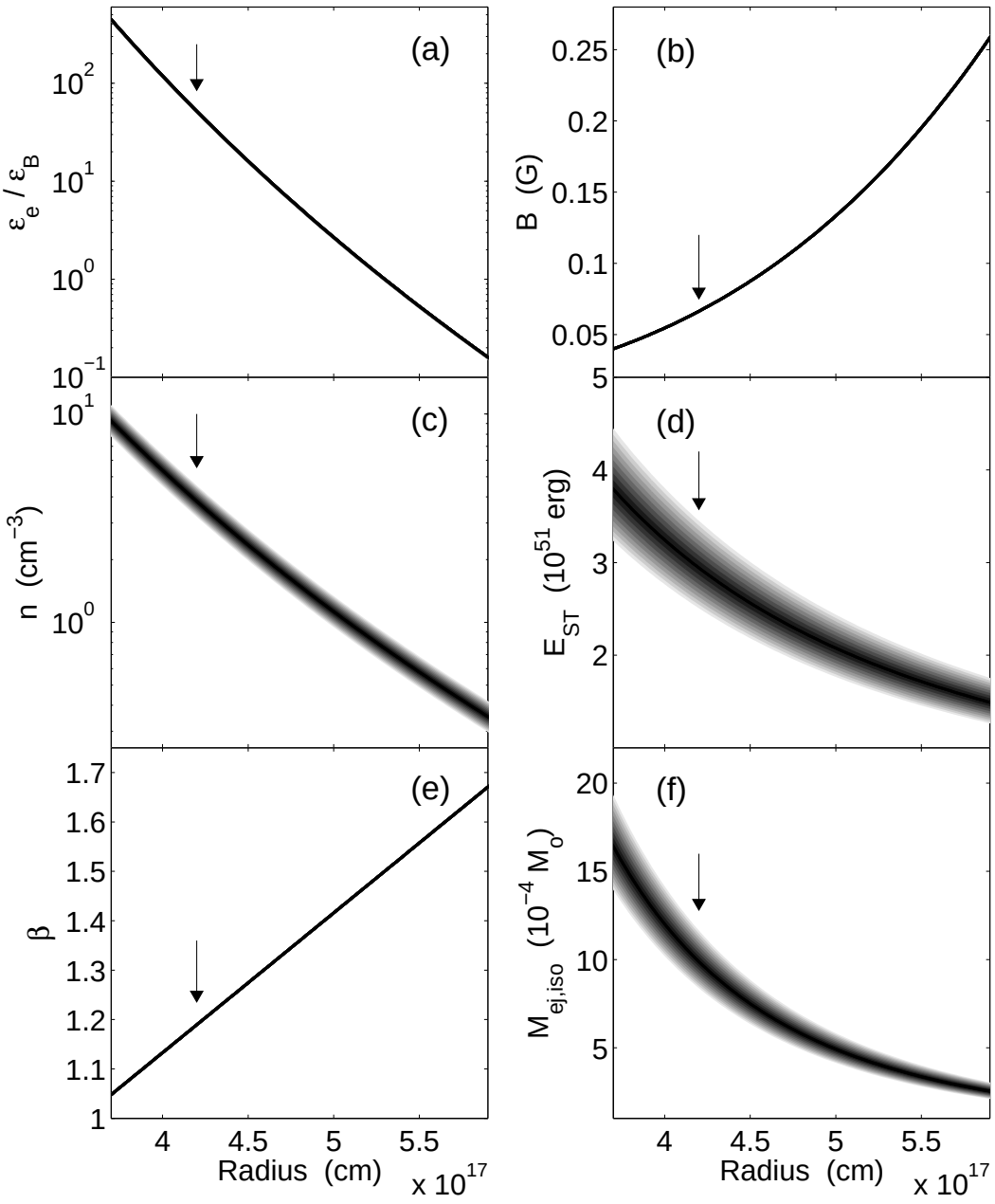

Figure 5.6: Physical parameters of the Sedov-Taylor blastwave for GRB 970508 at $t_{\rm NR} = 100$ d for the range of radii that obey the constraint $E_e + E_B \leq E_{\rm ST}/2$ (Figure 5.5): (a) The ratio of energy in the relativistic electrons to that in the magnetic fields, (b) the magnetic field strength, (c) the density of the circumburst medium, (d) the Sedov-Taylor energy, (e) the velocity of the blastwave, and (f) the isotropic-equivalent mass of the ejecta produced by the central engine and responsible for the afterglow emission. The arrows mark the most likely values using an estimate of the cooling frequency from a combination of the radio and optical data (§5.4 and Figure 5.5).

ejecta at early time. Both the optical and X-ray light curves of this burst exhibited a sharp increase in flux approximately 1 day after the burst, by a factor of about 4 and $\gtrsim 2$, respectively (Piro et al. 1998; Sokolov et al. 1998). The flux in these bands depends on energy as $F_\nu \propto E^{(p+3)/4}$ and $\propto E^{(p+2)/4}$, respectively (Sari et al. 1998). Thus, if we interpret the flux increase as due to injection of energy from ejecta with $\Gamma \sim 5 - 10$ (Panaitescu et al. 1998) we find an energy increase of about a factor of three. The analysis performed here provides an estimate of the total energy following the injection and thus

ϵ_γ appears to be low. The actual value of ϵ_γ is thus $\sim 10\%$.

Although GRBs 980703 and 970508 are currently the only bursts with sufficient radio data to warrant the full Sedov-Taylor analysis, flattening of radio light curves at late time have been noted in several other cases, most notably GRBs 980329, 991208, 000301C, 000418 and 000926 (Frail et al. 2004). Interpreting the flattening as a transition to non-relativistic expansion and using the expression for the flux at 8.5 GHz at the time of the transition, $F_\nu(t_{\rm NR}) \approx 50[(1+z)/2]^{-1/2}\epsilon_{e,-1}\epsilon_{B,-1}^{3/4}n_0^{3/4}E_{51}d_{28}^{-2}$ μJy (Livio & Waxman 2000), we find the rough results $n_0^{3/4}E_{51} \approx 6$ (980329), ≈ 4 (991208), ≈ 25 (000301C), ≈ 6 (000418), and ≈ 22 (000926). Thus, for typical densities, $\sim 1-10$ cm^{-3} (Panaitescu & Kumar 2002; Yost et al. 2003), the inferred kinetic energies are again of the order of $10^{51}-10^{52}$ erg.

This leads to the following conclusions. First, the energy scale of cosmological bursts is about 5×10^{51} erg, at least three orders of magnitude higher than the kinetic energies in fast ejecta determined for local type Ib/c SNe from radio observations (Berger et al. 2002b, 2003b), and an order of magnitude higher relative to the nearby ($d \approx 40$ Mpc) GRB 980425 associated with SN 1998bw (Kulkarni et al. 1998; Li & Chevalier 1999; **?**) and GRB 031203 ($z = 0.105$; Prochaska et al. 2004; Soderberg et al. 2004). Second, as already noted in the case of GRB 030329 (Berger et al. 2003c), there is a wide dispersion in the fraction of energy in ultra-relativistic ejecta, such that the γ-rays are a poor proxy for the total energy produced by the engine.

Thus, radio calorimetry is uniquely suited for addressing the relation between various cosmic explosions. So far, such studies reveal a common energy scale in relativistic ejecta of about 5 foe (foe $\equiv 10^{51}$ erg) for cosmological GRBs (Berger et al. 2003c), about 0.1 foe for the low redshift bursts (980425, 031203), and $\lesssim 10^{-3}$ foe in fast ejecta for type Ib/c SNe. The open question now is whether we are beginning to trace a continuum in the energetics of cosmic explosions, or whether the various classes truly represent distinct physical mechanisms with different energy scales. Fortunately, the best example to date of an object possibly bridging the various populations, GRB 030329, still shines brightly in the radio a year after the burst.

We thank Eli Waxman, Sarah Yost and Re'em Sari for valuable discussions, and the referee, Roger Chevalier, for useful comments. We acknowledge NSF and NASA grants for support.

Table 5.1. Physical Parameters of GRBs 980703 and 970508

Parameter	GRB 980703	GRB 970508
r (10^{17} cm)	$1.05 - 2.5$	$3.7 - 5.9$
B (G)	$0.02 - 0.7$	$0.04 - 0.25$
γ	$8 - 270$	$65 - 165$
n (cm^{-3})	$8 - 3.5 \times 10^3$	$0.4 - 10$
ϵ_e	$0.01 - 0.45$	$0.07 - 0.5$
ϵ_B	$5 \times 10^{-6} - 0.4$	$1 \times 10^{-3} - 0.45$
$M_{\rm ej,iso}$ (10^{-4} M$_\odot$)	$1 - 40$	$2 - 18$
$E_{\rm ST}$ (10^{50} erg)	$9 - 56$	$15 - 38$
$E_K(t_{\rm dec})$ (10^{51} erg)	4	30

Note. — Physical parameters of GRBs 980703 and 970508 derived from the non-relativistic evolution of their blastwaves. The range of allowed radii, and hence physical parameters, is determined by the condition $(E_e + E_B) \leq E_{\rm ST}/2$. The last entry in the table, $E_K(t_{\rm dec})$, is the total kinetic energy at the deceleration time, $t_{\rm dec} \approx 90$ s, including synchrotron radiative losses (§5.5).

CHAPTER 6

A Common Origin for Cosmic Explosions Inferred from Calorimetry of GRB 030329†

E. Berger[a], S. R. Kulkarni[a], G. Pooley[b], D. A. Frail[c], V. McIntyre[d], R. M. Wark[e], R. Sari[f], A. M. Soderberg[a], D. W. Fox[a], S. Yost[g], P. A. Price[h]

[a]Department of Astronomy, 105-24 California Institute of Technology, Pasadena, CA 91125, USA

[b]Mullard Radio Astronomy Observatory, Cavendish Lab., Madingley Road, Cambridge CB3 0HE, UK

[c]National Radio Astronomy Observatory, P. O. Box 0, Socorro, NM 87801

[d]Australia Telescope National Facility, CSIRO, P.O. Box 76, Epping, NSW 1710, Australia

[e]Australia Telescope National Facility, CSIRO, Locked Bag 194, Narrabri NSW 2390, Australia

[f]Theoretical Astrophysics 130-33, California Institute of Technology, Pasadena, CA 91125, USA

[g]Space Radiation Laboratory 220-47, California Institute of Technology, Pasadena, CA 91125, USA

[h]RSAA, ANU, Mt. Stromlo Observatory, via Cotter Rd, Weston Creek, ACT, 2611, Australia

Abstract

Past studies (Frail et al. 2001; Berger et al. 2003a; Bloom et al. 2003b) suggest that long-duration γ-ray bursts (GRBs) have a standard energy of $E_\gamma \sim 10^{51}$ erg in ultra-relativistic ejecta when corrected for asymmetry ("jets"). However, recently (Berger et al. 2003a; Bloom et al. 2003b) a group of sub-energetic bursts, including the peculiar GRB 980425 associated (Galama et al. 1998c) with SN 1998bw ($E_\gamma \approx 10^{48}$ erg), has been identified. Here we report radio observations of GRB 030329, the nearest burst to date, which allow us to undertake calorimetry of the explosion. Our observations require a two-component explosion: a narrow (5°) ultra-relativistic component responsible for the γ-rays and early afterglow, and a wide, mildly relativistic component responsible for the radio and optical afterglow beyond 1.5 days. While the γ-rays are energetically minor, the total energy release, dominated by the wide component, is similar (Frail et al. 2001; Berger et al. 2003a; Bloom et al. 2003b; Panaitescu & Kumar 2002) to that of other GRBs. Given the firm link (Stanek et al. 2003; Hjorth & et al. 2003) of GRB 030329 with SN 2003dh our result suggests a common origin for cosmic explosions in which, for reasons not understood, the energy in the highest velocity ejecta is highly variable.

† A version of this chapter was published in *Nature*, vol. 426, 154–157, (2003).

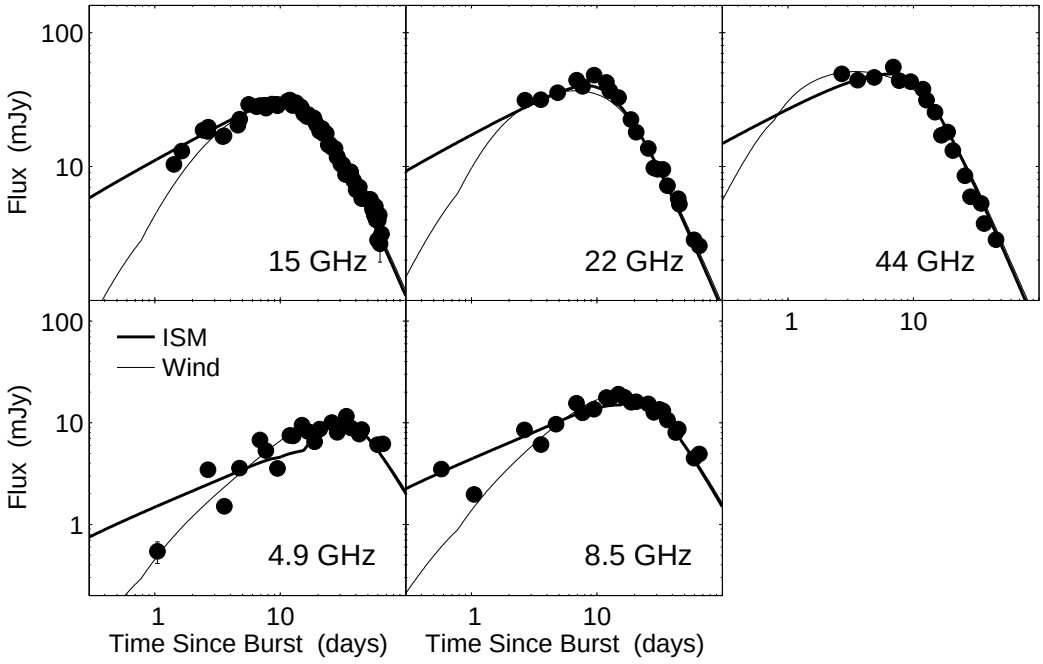

Figure 6.1: Radio light curves of the afterglow of GRB 030329. All measurements include 1σ error bars which in most cases are smaller than the symbols. The data are summarized in Tables 6.1 and 6.2. The solid lines are models of synchrotron emission from collimated relativistic ejecta expanding into uniform (thick) and wind (thin) circumburst media.

SECTION 6.1

Radio Observations of GRB 030329

We initiated observations of the nearby GRB 030329 ($z = 0.1685$) in the centimeter band with the Very Large Array (VLA) approximately 13.8 hours after the burst, on March 30.06 UT. A single 7-hour observation was obtained with the Australia Telescope Compact Array (ATCA) on Mar. 30.53 UT. Radio observations at 15.3 GHz made with the Ryle Telescope at Cambridge (UK). The log of the observations and the resulting light curves are displayed in Tables 6.1 and 6.2 and Figure 6.1.

In the initial observation we detect a point source at right ascension $\alpha(\mathrm{J2000})=10^{\mathrm{h}}44^{\mathrm{m}}49.95^{\mathrm{s}}$, and declination $\delta(\mathrm{J2000})=21^{\circ}31'17.38''$, with an uncertainty of about 0.1 arcsec in each coordinate, consistent with the position of the optical counterpart.

In all VLA observations we used the standard continuum mode with 2×50 MHz bands. At 22.5 and 43.3 GHz we used referenced pointing scans to correct for the systematic $10 - 20$ arcsec pointing errors of the VLA antennas. We used the extra-galactic sources 3C 147 (J0542+498) and 3C 286 (J1331+305) for flux calibration, while the phase was monitored using J1111+199 at 1.43 GHz and J1051+213 at all other frequencies. The ATCA observations were performed at 4.80, 6.21, 8.26, and 9.02 GHz with a bandwidth of 64 MHz in each frequency. The phase was monitored using J1049+215, while the flux was calibrated using J1934-638. The data were reduced and analyzed using the Astronomical Image Processing System (VLA) and the Multichannel Image Reconstruction, Image Analysis and Display package (ATCA). The flux density and uncertainty were measured from the resulting maps by fitting a Gaussian model to the afterglow. In addition to the rms noise in each measurement we estimate a systematic uncertainty of about 2% due to uncertainty in the absolute flux calibration.

All observations with the Ryle telescope were made by interleaving 15 minutes scans of GRB 030329 with 2.5 minutes scans of the phase calibrator J1051+2119. The absolute flux scale was calibrated using 3C 48 and 3C 286. We used 5 antennas providing 10 baselines in the range 35 – 140 m. Since the position of the source is well known the in-phase component of the vector sum of the 10 baselines was

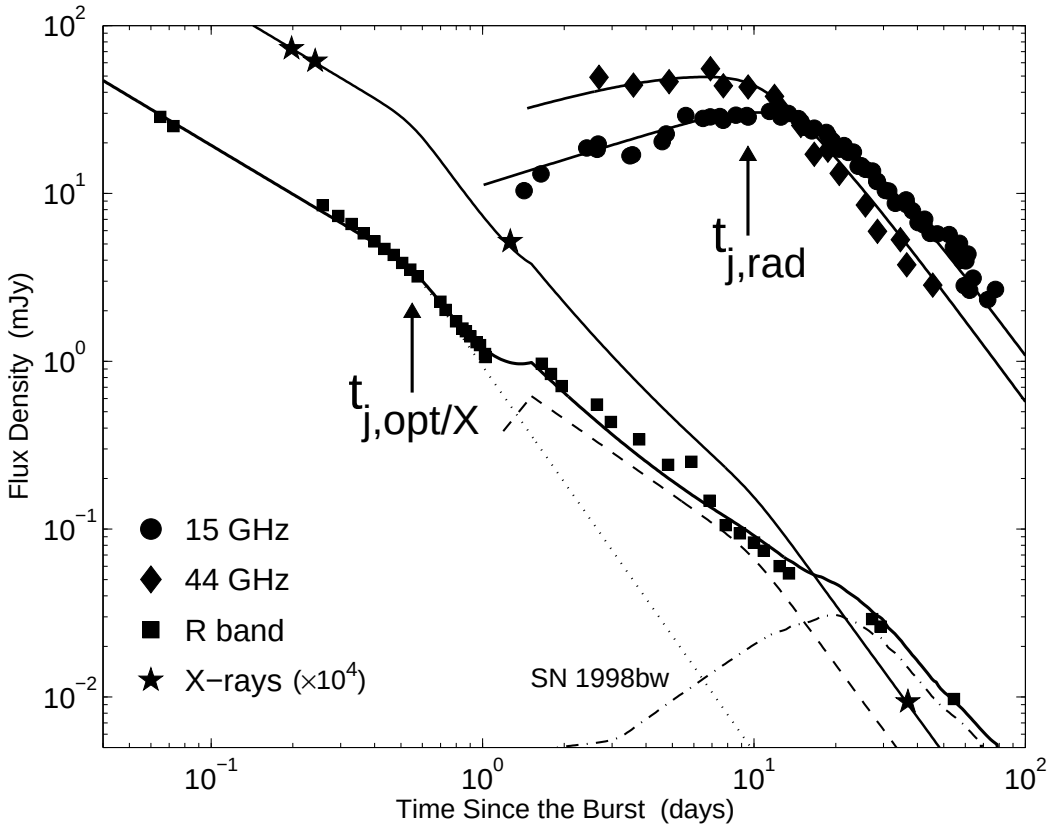

Figure 6.2: Radio to X-ray light curves of the afterglow of GRB 030329. The optical data, from Price et al. (2003) and the GRB Coordinates Network (Henden et al. 2003; Ibrahimov et al. 2003; Testa et al. 2003), have been corrected for Galactic extinction, $A_R = 0.067$ mag. The dotted line is the model proposed by Price et al. (2003) for the early optical emission, with $t_{j,\rm opt} \approx 0.55$ d. The dashed line is an extapolation of our uniform density model to the optical R-band. The model in the X-ray band is based on the measured (Tiengo et al. 2003) optical to X-ray spectral slope and an extapolation of our uniform density model. The sharp increase in the optical flux at $t \lesssim 1.5$ d is due to the deceleration of the slower second jet component. Finally, the dot-dashed line is the optical emission from SN 1998bw at the redshift of GRB 030329, $z = 0.1685$, used as a proxy for SN 2003dh (Stanek et al. 2003).

used as an unbiased estimate of the flux density. The typical rms fluctuation on the signal in a 32-s integration period is approximately 6 mJy. We also add a systematic uncertainty of about 2% due to uncertainty in the absolute flux calibration.

The afterglow was also observed extensively in the millimetre (100 GHz) and sub-millimetre (250 GHz) bands (Sheth et al. 2003). While this is the brightest radio afterglow detected to date, the low redshift results in a peak luminosity, $L_{\nu,p}(8.5\,{\rm GHz}) \approx 1.8 \times 10^{31}$ erg s^{-1} Hz^{-1}, typical (Frail et al. 2003a) of other long-duration GRBs.

SECTION 6.2

Broad-band Afterglow Models

The observed rapid decline, $F_\nu \propto t^{-1.9}$ at $t \gtrsim 10$ d and the decrease in peak flux at $\nu \lesssim 22.5$ GHz (Figure 6.1) are the hallmarks of a collimated explosion. In this framework (Sari et al. 1999), the sharp decline (or "jet break") occurs at the time, t_j, when $\Gamma(t_j) \sim \theta_j^{-1}$ due to relativistic abberation ("beaming") and rapid side-ways expansion; here Γ is the bulk Lorentz factor and θ_j is the opening angle of the jet.

We model the afterglow emission (e.g., Berger et al. 2000; Panaitescu & Kumar 2002) from 4.9 to 250

GHz assuming a uniform (Sari et al. 1999) as well as a "wind" (Chevalier & Li 2000) (particle density profile, $\rho \propto r^{-2}$, where r is the distance from the source) circumburst medium. We find $\chi^2_r = 31.3$ and 39.8 (164 degrees of freedom) for the uniform density and wind models, respectively; these include a 2% systematic error added in quadrature to each measurement. The large values of χ^2_r are dominated by interstellar scintillation (ISS) at $\nu \lesssim 15$ GHz and mild deviations from the expected smooth behavior at the high frequencies. Comparing the data and models, we find rms flux modulations of 0.25 at 4.9 GHz, 0.15 at 8.5 GHz, and 0.08 at 15 GHz, as well as a drop by a factor of three in the level of modulation from ~ 3 to 40 days. These properties are expected in weak ISS as the fireball expands on the sky. The inferred source size of about 20 μas (i.e., $\sim 2 \times 10^{17}$ cm) at $t \sim 15$ days is in close agreement with theoretical expectations (Galama et al. 2003).

In the uniform density model the jet break occurs at $t \approx 10$ d corresponding to an opening angle, $\theta_j \approx 0.3$ (17°). From the derived synchrotron parameters (at $t = t_j$): $\nu_a \approx 19$ GHz, $\nu_m \approx 43$ GHz, $F_{\nu,m} \approx 96$ mJy we find an isotropic kinetic energy, $E_{K,\rm iso} \approx 5.6 \times 10^{51} \nu_{c,13}^{1/4}$ erg, a circumburst density $n = 1.8 \nu_{c,13}^{3/4}$ cm^{-3}, and the fractions of energy in the relativistic electrons and magnetic field of $0.16 \nu_{c,13}^{1/4}$ and $0.10 \nu_{c,13}^{-5/4}$, respectively; here $\nu_c = 10^{13} \nu_{c,13}$ is the synchrotron cooling frequency, and a constraint on Inverse Compton cooling as advocated by Sari & Esin (Sari & Esin 2001) indicates $\nu_{c,13} \lesssim 1$. The beaming-corrected kinetic energy is $E_K \approx 2.5 \times 10^{50} \nu_{c,13}^{1/4}$ erg, typical of other well-studied long-duration GRBs (Panaitescu & Kumar 2002). The parameters derived from the wind model are consistent with those from the uniform density model to within 10%.

Thus, neither model is strongly preferred, but $t_{j,\rm rad} \approx 9.8$ d is required (Figure 6.1).

SECTION 6.3

A Two-Component Jet

Using the inferred particle density of $n \approx 1.8$ cm^{-3} and assuming a γ-ray efficiency, $\epsilon_\gamma = 0.2$ (Bloom et al. 2003b) we infer $\theta_{j,\rm rad} \sim 0.3$ rad, or 17°. The kinetic energy in the explosion corrected for collimation is $E_K = f_b E_{K,\rm iso} \approx 2.5 \times 10^{50}$ erg, where $f_b = [1 - \cos(\theta_j)]$ is the beaming fraction and $E_{K,\rm iso}$ is the isotropic equivalent kinetic energy. This value is comparable to that inferred from modeling of other afterglows (Panaitescu & Kumar 2002).

In contrast to the above discussion, Price et al. (2003) note a sharp break in the optical afterglow at $t = 0.55$ d (Figure 6.2). The X-ray flux (Tiengo et al. 2003) tracks the optical afterglow for the first day, with a break consistent with that seen in the optical. Thus the break at 0.55 d is not due to a change in the ambient density since for typical parameters (Kumar 2000; Freedman & Waxman 2001) the X-ray emission is not sensitive to density. However, unlike the optical emission the X-ray flux at later times continues to decrease monotonically. Thus we conclude that there are two emitting components: one responsible for the early optical and X-ray emission and the other responsible for the optical emission beyond 1.5 days.

The first component, given the characteristic t^{-2} decay for both the X-ray and optical emission, is reasonably modeled by a jet. For the parameters used above (n, ϵ_γ) the opening angle is 0.09 rad or 5°.

The resurgence in the optical emission at 1.5 d requires a second component. An increase in the ambient density cannot explain this resurgence since the predicted decrease in radio luminosity, arising from the increase in synchrotron self-absorption, is not observed (Figure 6.1). An increase in the energy of the first component, for example by successive shells with lower Lorentz factors as advocated by Granot et al. (Granot et al. 2003), is ruled out by the lack (Sheth et al. 2003) of strong radio or millimetric emission expected (Sari & Mészáros 2000) from reverse shocks.

Thus, by a process of elimination, we are led to a two-component explosion model in which the first component (a narrow jet, 5°) with initially larger Γ is responsible for the γ-ray burst and the early optical and X-ray afterglow including the break at 0.55 d, while the second component (a wider jet, 17°) powers the radio afterglow and late optical emission (Figure 6.2). The break due to the second

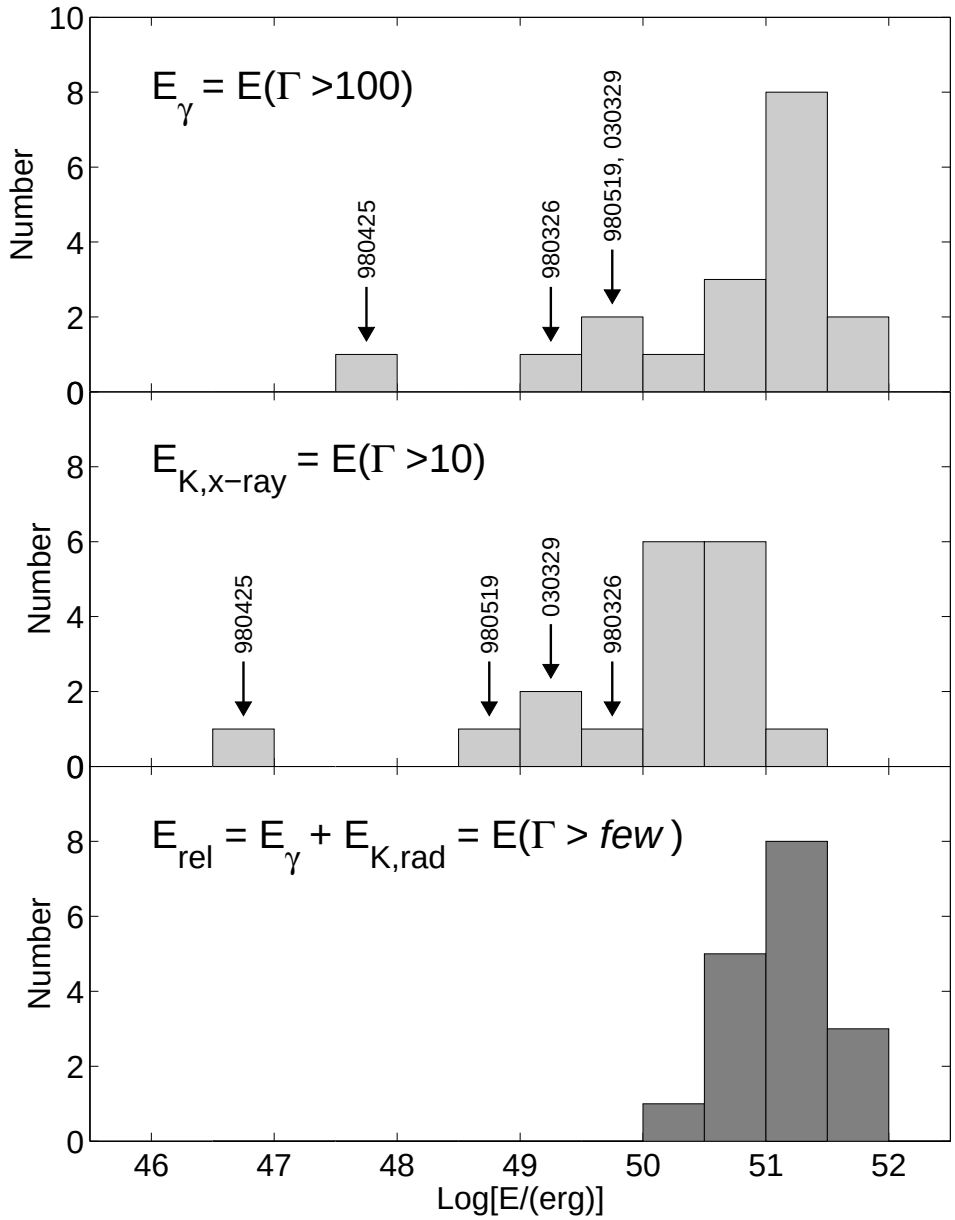

Figure 6.3: Histograms of various energies measured for GRBs: the beaming-corrected γ-ray energy, E_γ, the kinetic energy inferred from X-rays at $t = 10$ hr, $E_{K,X}$, and the total relativistic energy, $E_{\rm rel} = E_\gamma + E_K$, where E_K is the beaming-corrected kinetic energy inferred (Li & Chevalier 1999; Panaitescu & Kumar 2002) from the broad-band afterglow. The significantly wider dispersion in E_γ and $E_{K,X}$ as compared to the total explosive yield indicates that engines in cosmic explosions produce approximately the same quantity of energy (thus pointing to a common origin), but the quality of these engines, as indicated by ultra-relativistic output, varies widely.

component is readily seen in the radio afterglow, but is masked by SN 2003dh in the optical bands, thus requiring careful subtraction (Figure 6.2). Such a two-component jet finds a natural explanation in the collapsar model (MacFadyen et al. 2001).

The beaming-corrected γ-ray energy, emitted by the narrow jet, is only $E_\gamma \approx 5 \times 10^{49}$ erg, significantly lower than the strong clustering (Bloom et al. 2003b) around 1.3×10^{51} erg seen in most bursts. Similarly, the beaming-corrected X-ray luminosity (Tiengo et al. 2003) at $t = 10$ hours, a proxy for the kinetic energy of the afterglow on that timescale, is $L_{X,10} \approx 3 \times 10^{43}$ erg s^{-1}, a factor of ten below the tightly clustered values (Berger et al. 2003a) for most other bursts. However, the second component, which is mildly relativistic (as determined by the lower energy peak of its spectrum), carries the bulk

of the energy, as indicated by our modeling of the radio emission. We note that our model, with the energy in the lower Lorentz factor component dominating over the narrow ultra-relativistic component, is not consistent with "universal standard jet" model (Rossi et al. 2002).

SECTION 6.4

A Common Origin for Cosmic Explosions

The afterglow calorimetry presented here has important ramifications for our understanding of GRB engines. Recently, we have come to recognize a sub-class of cosmological GRBs marked by rapidly fading afterglows at early time (i.e., similar to GRB 030329). These events are sub-energetic (Berger et al. 2003a; Bloom et al. 2003b) in E_γ and early X-ray afterglow luminosity. However, as demonstrated by our calorimetry of GRB 030329, such bursts may have total explosive yields similar to other GRBs.

In Figure 6.3 we plot E_γ (Bloom et al. 2003b), the kinetic energy inferred from X-rays at $t = 10$ hr (Berger et al. 2003a), $E_{K,X}$, and the total relativistic energy, $E_{\rm rel} = E_\gamma + E_K$, where E_K is the beaming-corrected kinetic energy inferred (Li & Chevalier 1999; Panaitescu & Kumar 2002) from the broad-band afterglow. The energy in X-rays is determined using $E_{K,X} = L_X t/\epsilon_e(\alpha_X - 1)$, with $t = 10$ hr, $\epsilon_e = 0.1$, and $\alpha_X = 1.3$ is the median decay rate in the X-ray band. For GRB 980519 we find that the evolution of the radio emission requires a much wider jet, $\theta_j \sim 0.3$, than what is inferred from the optical, $\theta_j \sim 0.05$; here we assume $z = 1$. We therefore infer $E_K \sim 2 \times 10^{50}$ erg from the radio data compared to $E_\gamma \approx 4 \times 10^{49}$ erg. The γ-ray energy of GRB 980425 is an upper limit since the degree of collimation is not known. For the kinetic energy we use the value derived by Li & Chevalier (1999) based on the radio evolution of SN 1998bw. There is a significantly wider dispersion in E_γ and $E_{K,X}$ as compared to the total explosive yield.

This leads to the following conclusions. First, radio calorimetry, which is sensitive to all ejecta with $\Gamma \gtrsim few$, shows that the explosive yield of the nearest "classical" event, GRB 030329, is dominated by mildly relativistic ejecta. Ultra-relativistic ejecta which produced the γ-ray emission is energetically unimportant. Second, the total energy yield of GRB 030329 is similar to those estimated for other bursts. Along these lines, the enigmatic GRB 980425 associated (Galama et al. 1998c) with the nearby supernova SN 1998bw also has negligible γ-ray emission, $E_{\gamma,\rm iso} \approx 8 \times 10^{47}$ erg; however, radio calorimetry (Li & Chevalier 1999) shows that even this extreme event had a similar explosive energy yield (Figure 6.3). The newly recognized class of cosmic explosions, the X-ray Flashes (Heise et al. 2003), exhibits little or no γ-ray emission but appear to have comparable X-ray and radio afterglows to those of GRBs. Thus, the commonality of the total energy yield indicates a common origin, but apparantly the ultra-relativistic output is highly variable. Unraveling what physical parameter is responsible for the variation in the "purity" (ultra-relativistic output) of the engine appears to be the next frontier in the field of cosmic explosions.

GRB research at Caltech is supported in part by funds from NSF and NASA. We are, as always, indebted to Scott Barthelmy and the GCN. The VLA is operated by the National Radio Astronomy Observatory, a facility of the National Science Foundation operated under cooperative agreement by Associated Universities, Inc. The Australia Telescope is funded by the Commonwealth of Australia for operations as a National Facility managed by CSIRO. The Ryle Telescope is supported by PPARC.

Table 6.1. Very Large Array Radio Observations of GRB 030329

Epoch UT	Δt (days)	$F_{1.43}$ (mJy)	$F_{4.86}$ (mJy)	$F_{8.46}$ (mJy)	$F_{15.0}$ (mJy)	$F_{22.5}$ (mJy)	$F_{43.3}$ (mJy)
Mar 30.06	0.58	—	—	3.50 ± 0.06	—	—	—
Mar 30.53	1.05	—	0.54 ± 0.13	1.98 ± 0.17	—	—	—
Apr 1.13	2.65	< 0.21	3.45 ± 0.05	8.50 ± 0.05	19.68 ± 0.14	30.40 ± 0.06	46.63 ± 0.18
Apr 2.05	3.57	< 0.30	1.51 ± 0.05	6.11 ± 0.04	16.98 ± 0.19	31.59 ± 0.14	44.17 ± 0.35
Apr 3.21	4.76	< 0.36	3.58 ± 0.04	9.68 ± 0.03	22.59 ± 0.12	35.57 ± 0.09	46.32 ± 0.23
Apr 5.37	6.89	< 0.40	6.77 ± 0.08	15.56 ± 0.06	28.58 ± 0.20	44.09 ± 0.15	55.33 ± 0.43
Apr 6.16	7.68	< 0.25	5.34 ± 0.10	12.55 ± 0.21	27.26 ± 0.21	39.68 ± 0.20	43.81 ± 1.00
Apr 7.97	9.49	< 0.68	3.55 ± 0.11	13.58 ± 0.09	28.50 ± 0.23	48.16 ± 0.23	43.06 ± 1.33
Apr 10.38	11.90	< 0.58	7.51 ± 0.08	17.70 ± 0.05	31.40 ± 0.25	42.50 ± 0.14	37.86 ± 0.46
Apr 11.17	12.69	—	7.42 ± 0.09	17.28 ± 0.10	29.60 ± 0.29	36.84 ± 0.16	31.26 ± 0.51
Apr 13.35	14.87	—	9.49 ± 0.13	19.15 ± 0.08	26.78 ± 0.33	32.69 ± 0.13	25.44 ± 0.51
Apr 15.14	16.66	—	8.21 ± 0.08	17.77 ± 0.10	24.50 ± 0.31	—	17.10 ± 0.71
Apr 17.20	18.72	< 0.63	6.50 ± 0.11	15.92 ± 0.07	22.02 ± 0.25	22.41 ± 0.08	18.07 ± 0.28
Apr 19.06	20.58	—	8.66 ± 0.10	16.08 ± 0.06	18.35 ± 0.24	18.03 ± 0.11	13.15 ± 0.29
Apr 24.18	25.70	—	10.04 ± 0.08	15.34 ± 0.06	13.93 ± 0.26	13.63 ± 0.13	8.54 ± 0.48
Apr 26.92	28.44	< 0.58	8.05 ± 0.08	12.67 ± 0.09	11.82 ± 0.26	9.75 ± 0.23	5.95 ± 0.62
Apr 28.96	30.48	—	—	—	10.40 ± 0.33	9.53 ± 0.21	—
Apr 29.99	31.51	—	9.80 ± 0.09	13.55 ± 0.07	—	—	—
May 2.06	33.58	—	11.62 ± 0.08	13.10 ± 0.06	—	9.52 ± 0.14	—
May 3.07	34.59	—	—	—	—	—	5.30 ± 0.32
May 5.00	36.52	—	8.90 ± 0.08	10.64 ± 0.06	8.58 ± 0.17	7.20 ± 0.09	3.75 ± 0.26
May 11.03	42.55	—	7.72 ± 0.13	8.04 ± 0.08	7.03 ± 0.19	—	—
May 13.03	44.55	—	8.57 ± 0.09	8.68 ± 0.08	5.77 ± 0.22	5.75 ± 0.10	—
May 14.00	45.52	—	—	—	—	5.23 ± 0.17	2.84 ± 0.23
May 28.03	59.55	—	6.08 ± 0.10	4.48 ± 0.09	2.82 ± 0.21	2.84 ± 0.20	—
June 4.01	66.53	1.94 ± 0.06	6.20 ± 0.08	4.93 ± 0.06	—	2.56 ± 0.12	—

Note. — The columns are (left to right), (1) Epoch of observation, (2) time since the burst, and (3-8) measured flux densities at 1.43 through 43.3 GHz.

Table 6.2. Ryle Telescope Radio Observations of GRB 030329

Epoch UT	Δt (days)	$F_{15.3}$ (mJy)	Epoch UT	Δt (days)	$F_{15.3}$ (mJy)
Mar 30.91	1.43	10.38 ± 0.28	Apr 21.72	23.24	17.63 ± 0.29
Mar 31.12	1.64	13.05 ± 0.28	Apr 22.66	24.18	14.51 ± 0.49
Mar 31.91	2.43	18.66 ± 0.28	Apr 23.33	24.85	14.62 ± 0.49
Apr 1.12	2.64	18.29 ± 0.28	Apr 25.81	27.33	13.60 ± 0.65
Apr 1.98	3.50	16.75 ± 0.27	Apr 26.82	28.34	11.78 ± 0.52
Apr 3.07	4.59	20.36 ± 0.45	Apr 29.82	31.34	10.35 ± 0.49
Apr 4.09	5.61	29.13 ± 0.52	May 1.63	33.15	8.73 ± 0.52
Apr 4.97	6.49	27.97 ± 0.26	May 4.80	36.32	9.15 ± 0.50
Apr 5.97	7.49	28.69 ± 0.26	May 6.83	38.35	7.87 ± 0.50
Apr 7.06	8.58	29.29 ± 0.49	May 8.73	40.25	6.70 ± 0.50
Apr 7.89	9.41	29.15 ± 0.44	May 10.76	42.28	6.49 ± 0.50
Apr 9.89	11.41	30.78 ± 0.51	May 15.76	47.28	5.74 ± 0.50
Apr 11.05	12.57	28.52 ± 0.51	May 20.70	52.22	5.69 ± 0.53
Apr 11.88	13.40	29.92 ± 0.44	May 22.76	54.28	4.78 ± 0.78
Apr 13.05	14.57	27.90 ± 0.44	May 24.76	56.28	4.31 ± 0.55
Apr 13.87	15.39	24.74 ± 0.44	May 25.56	57.08	5.04 ± 0.84
Apr 14.82	16.34	23.60 ± 0.32	May 26.75	58.27	3.99 ± 0.63
Apr 16.96	18.48	23.06 ± 0.24	May 28.76	60.28	3.96 ± 0.58
Apr 17.92	19.44	20.51 ± 0.24	May 29.82	61.34	4.35 ± 0.50
Apr 19.95	21.47	19.27 ± 0.38	May 30.76	62.28	2.65 ± 0.72
Apr 20.72	22.24	17.53 ± 0.33	June 2.54	64.06	3.13 ± 0.76

Note. — The columns are (left to right), (1) Epoch of observation, (2) time since the burst, and (3) measured flux densitat 15.3 GHz.